

Study of charge changing cross sections for heavy ions in various medium and their applications in cosmic rays detection and hadrontherapy

By

Ashavani Kumar

Department of Physics



राष्ट्रीय प्रौद्योगिकी संस्थान कुरुक्षेत्र
National Institute of Technology Kurukshetra

OUTLINES

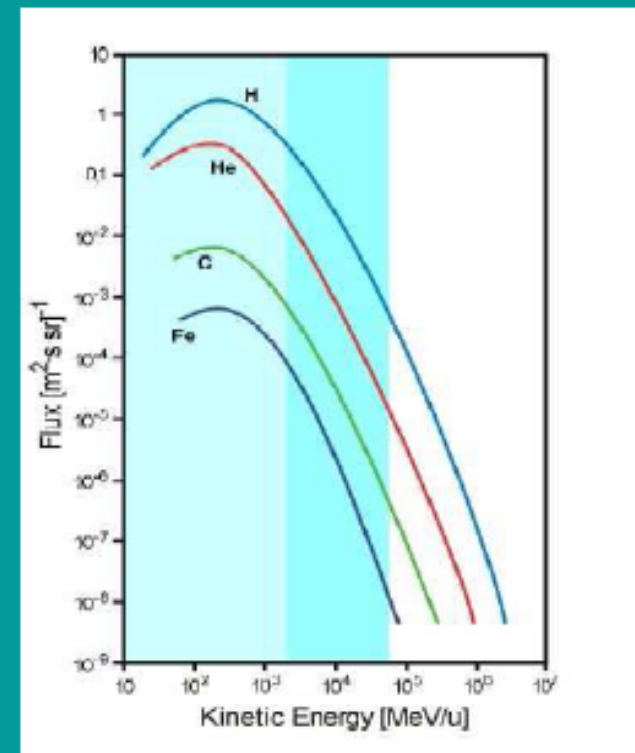
- **Introduction**
- **Nuclear Fragmentation**
- **Space Radiations**
- **Hadrontherapy**
- **Geant4: a simulation tool**
- **Applications**
- **Models incorporated in the present study**
- **Simulated Results**
- **Experimental setup for NTDs**
- **Charge Changing Cross-Section**
- **Charge Resolution**
- **Summary**
- **Publications & References**

- Radiation environment beyond low earth orbit (LEO) is not known very well and experimental data are sparse.
- Nuclear fragmentation represents an important problem for understanding the cosmic radiation, their origin as well as for shielding in spacecrafts and treatment plans in hadrontherapy.
- The use of high energy ions (Carbon, Oxygen, Neon and Silicon etc.) in cancer radiation therapy has grown considerably in recent years because ions heavier than protons show an improved dose distribution and an increasing biological effect (RBE) at the end of range (Bragg Peak).
- As compared to the measurements of fragmentation in different target materials made by electronic detectors, track etch detector technique is able to provide better information about fluence and fragmentation.
- The present work is an advancement in the study of high energy ions interactions with matter and nuclear fragmentations by using Nuclear Track Detectors (NTDs). The great interest for Fe, Si and C ions have attracted a number of experiments for galactic cosmic radiation (GCR) studies and in biology and physics at accelerator facilities reaching energies of the order of GeV/n.
- The Geant4 is one of the most effective tool for Monte Carlo (MC) simulation studies in cosmic rays interactions in various medium as well as for charge production studies etc.

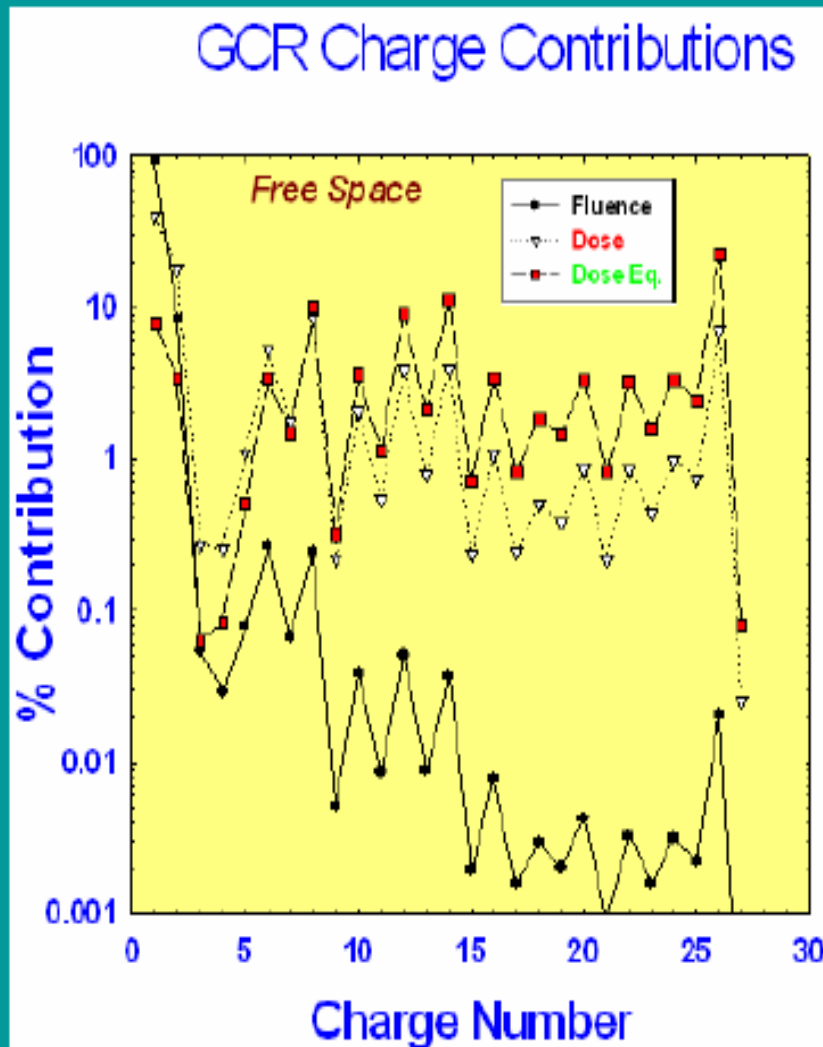
- **High-energy heavy projectiles will provide information on the behavior of high-density nuclear matter at high temperature.**
- **The projectile fragmentation for ultra-heavy nuclei in different elements allows indirectly to derive the partial cross-sections.**
- **Investigation of the charge pickup phenomena to the heaviest nuclei.**
- **The threshold energy of the limiting fragmentation phenomena has to be explored.**
- **By varying the energy during the irradiation in a well controlled manner one can superimpose many narrow Bragg peaks and obtain a Spread Out Bragg Peak (SBOP).**
- **Problems are usually challenged by resorting to computer codes able to simulate the nuclear interactions like; HIBRAC, HZETRN, PHITS, FLUCA and GEANT4 etc.**
- **However, these codes are affected by large uncertainties caused by lack of sufficient data concerning nuclear fragmentation cross sections at various energies.**
- **CR39 NTDs provide fragmentation cross sections for projectiles with $Z \geq 5$ in different targets.**
- **A charge resolution better than 0.2e can be easily achieved by CR39**

Radiation field in Space

- **Trapped radiation:** Van Allen belts (electrons, protons up to 600 MeV)
- **Solar radiation:** about 90% protons, $E < 1$ GeV, seldom but potentially dangerous (high dose) events
- **Galactic Cosmic Radiation (GCR):**
 - 2% electrons and positrons
 - 98% particles :
 - 87% protons
 - 12% α particles
 - 1% heavier ions (HZE particles)



Galactic Cosmic Ray charge contribution*



Dose eq. on **Earth**: 10 μ Sv/d

Dose eq. on **Mars**: 100-200 mSv/d

Dose eq. on **Moon**: 300-400 mSv/d

Dose eq. from **GCR**: 1 mSv/d

Hadron-therapy: Why Ion/Proton Beam?

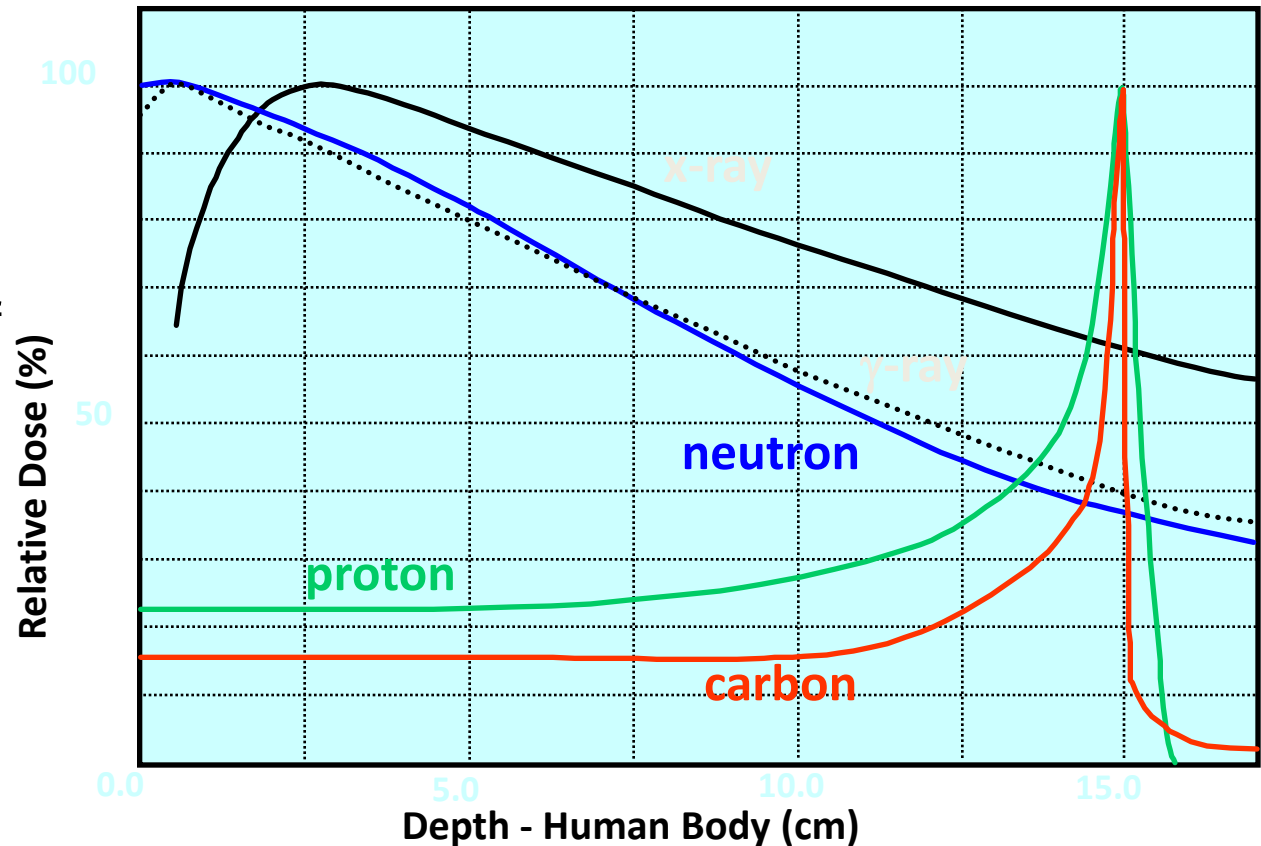
The Bragg peak provides an excellent dose distribution which is effective to deep-seated tumors.

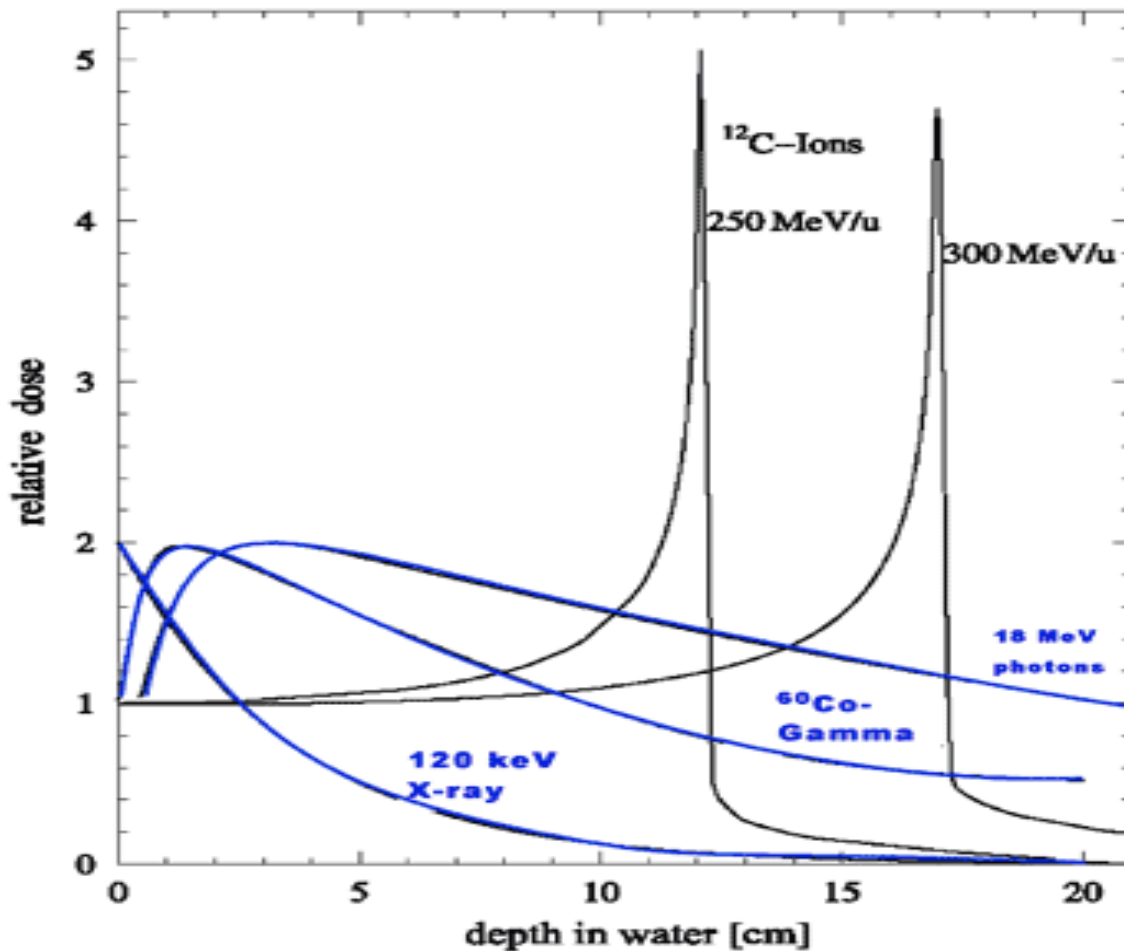
- A sharp peak of energy deposition at the end of the range.
- The sharp fall-off of the Bragg peak
 - A small range straggling

[Note]

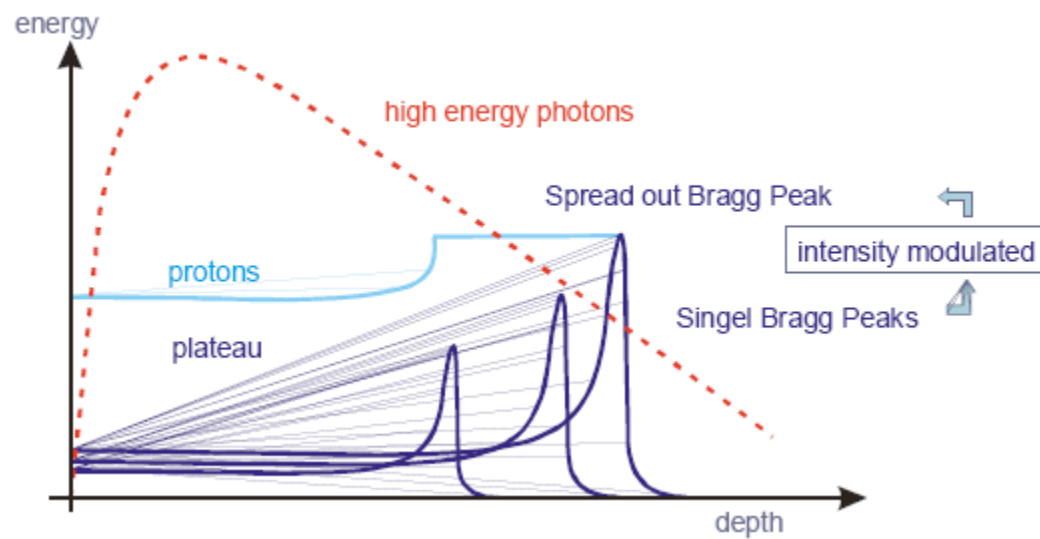
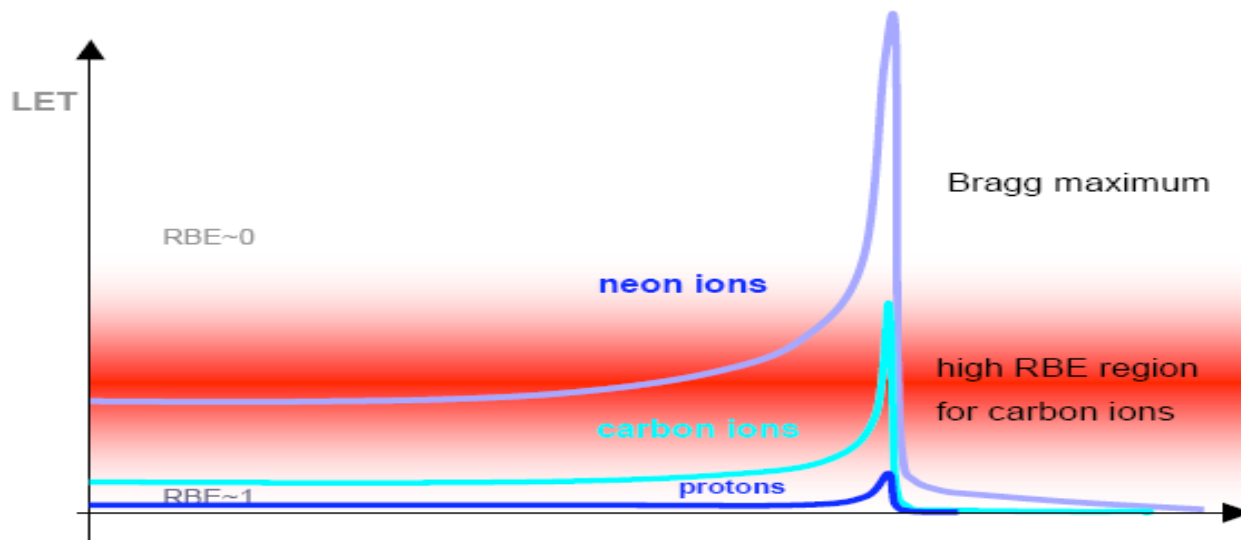
- Carbon has a tail after the Bragg peak.

Ref. <http://www.nirs.go.jp/tiryo/himac/himac2.htm>





Comparison of depth dose distribution in water as tissue equivalent. Ions have a peaked profile which allows greater dose at the tumor and lower dose to the normal tissue around. Changing the ion energy, one can shift in the depth position for energy deposition.



- **Hadron beams have an inverse dose profile that produces a greater dose to the tumor than to the healthy tissues in the entrance**
- **With the most advanced technique, Intensity Modulated Particle Therapy (IMPT), where the pencil of hadron beams is guided according to the shape of the zone to be treated, the tumor can be delineated in all its contours with a precision of 2-3 mm.**
- **Because of higher atomic numbers, the lateral and range scattering is much smaller for carbon or neon ions than for protons. One of the major advantages of heavy ion tumor therapy is the increase in relative biological effectiveness (RBE) of particle beams in particular at the end of their penetration depth, i.e. in the tumor volume. This increased effectiveness has to be taken into account for treatment planning. The RBE cannot be represented by a single number, but depends in a complex way on different factors like e.g. ion type and energy, depth in tissue, dose level and the tissue type. For applications of ion beams in tumor therapy, the increased RBE requires a corresponding general reduction in dose.**

In general, ions are better for radio-resistant tumors while ions minimize the risk of appearance of secondary tumors.

DISADVANTAGE OF CARBON IONS

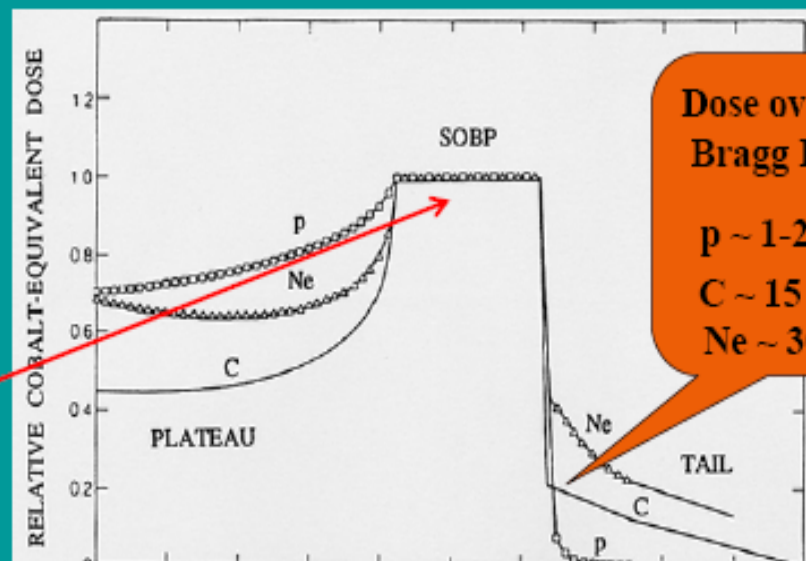
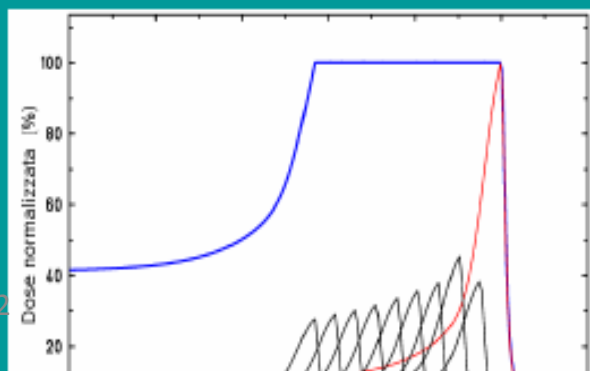
Nuclear Fragmentation of ^{12}C beam in the interaction processes with:

- *energy degraders,*
- *biological tissues*

Further problem \longrightarrow different biological effectiveness of the fragments

Mitigation and attenuation of the primary beam

Production of fragments with higher range vs primary ions



Dose over the Bragg Peak :

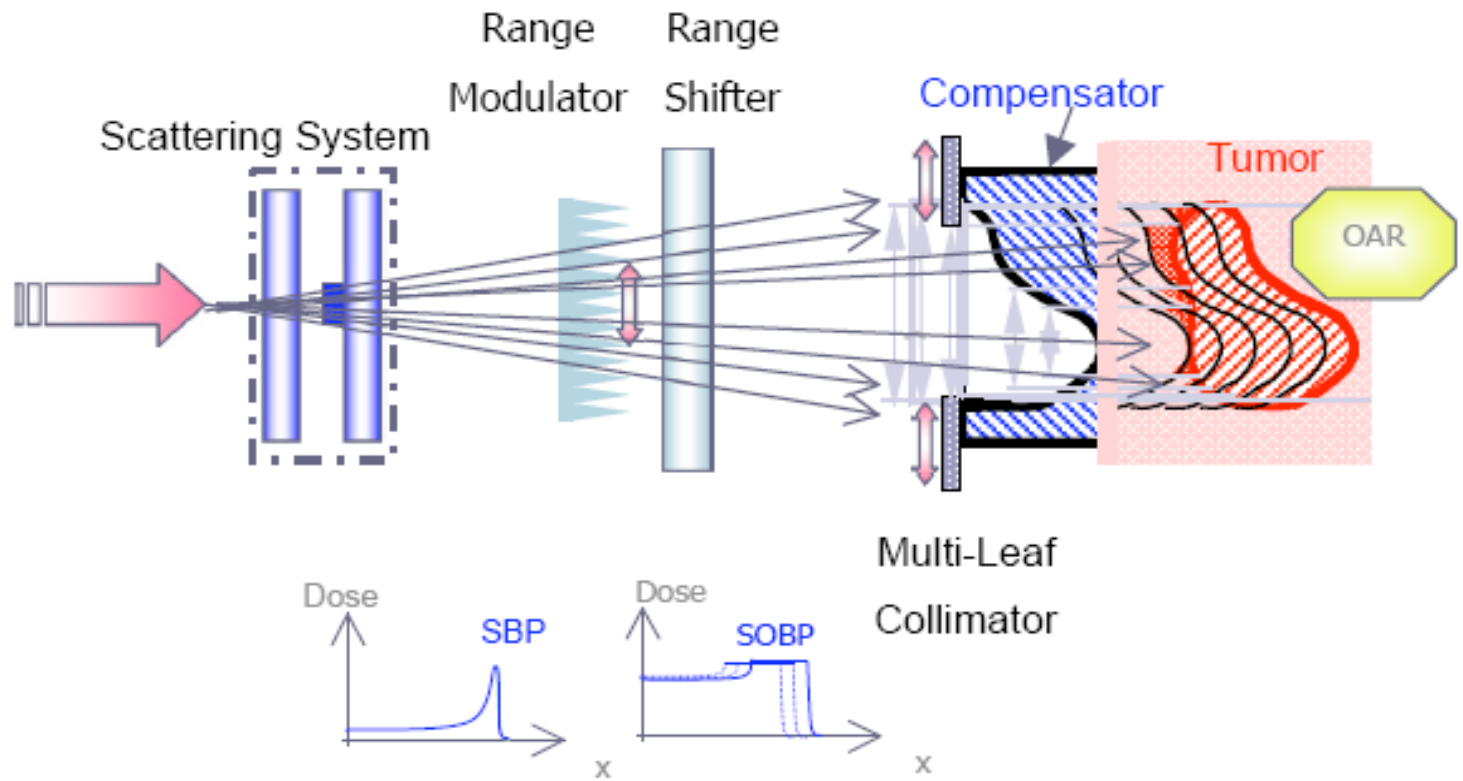
- p ~ 1-2 %
- C ~ 15 %
- Ne ~ 30 %

Monte Carlo for Hadrontherapy

- Dose distribution verification also in particular configurations
(where the measure is not possible)
- Treatment planning verification and/or commissioning
- Test of dosimetric systems (detectors, dose calculation theories, etc)
- Beam line transport optimization and verification
- RBE determination
- Tissue inhomogeneities by using specific material properties
- Secondary particles can be tracked

Monte Carlo can be considered today a very accurate approach for medical physics applications.





Geant4 is a toolkit for the simulation of the passage of particles through matter. Its areas of **application** include high energy, nuclear and accelerator physics, as well as studies in medical and space science.

The two main reference papers for Geant4 were published in ***Nuclear Instruments and Methods in Physics Research A* 506 (2003) 250-303** and ***IEEE Transactions on Nuclear Science* 53 No. 1 (2006) 270-278**. by CERN GEANT Group

Minimum Software Knowledge to Use Geant4

- **C++**

- Geant4 is implemented in C++, therefore a basic knowledge of C++ is mandatory
- C++ is a complex language, but you are not required to be a C++ expert to use Geant4

- **Object Oriented Technology**

- basic concepts
- in-depth knowledge needed only for the development of complex applications

- **Unix/Linux**

- Unix/Linux is a standard working environment for Geant4, therefore a minimum knowledge/experience is required
 - How to use basic Unix command
 - How to compile a C++ code

- **Windows**

- You can use Visual C++
- Though still you need some knowledge of Unix (cygwin) for installation

Brief introduction to the models used in present simulation study

Standard electromagnetic model

1. **Standard Electromagnetic model** is included in Geant4 as **G4EmStandard** model
 - a. This is used to study the energy loss of particles in medium.
 - b. This model contains the **definition** of all charged and uncharged particles.
 - c. **G4hMultiScattering** and **G4hIonisation** classes are included to describe energy loss due to multi-scattering and ionization processes.
 - d. While this model does not describe any type of **fragmentation** and does not produce secondary particles.

Processes included in Standard Electromagnetic physics model

Standard electromagnetic model has mainly two processes:

1. Ionization
2. Multiple scattering

Simulation of δ -rays

δ -rays with kinetic energies above a given threshold T_{cut} are explicitly considered for tracking.

Projectiles interact with quasi-free electrons in the medium and the differential collision cross-sections $d\sigma_{\delta}/dT$ for simulation is given by

$$\frac{d\sigma_{\delta}}{dT} = 2\pi r_e^2 m_e c^2 \frac{z_i^2 Z_2}{\beta^2} \frac{1}{T^2} \left[1 - \beta^2 \frac{T}{T_{\text{max}}} + \frac{T^2}{2E^2} \right]$$

where

r_e = electron radius

m_e = electron rest mass

β = particle velocity/speed of light

$z_i = \gamma Z_1$, Z_1 is atomic number of the ion

Stopping power algorithm

G4ionisation class of standard electromagnetic physics model uses stopping power algorithm

In algorithm,

below threshold (< 2 MeV/n), parameterized formula is used.

above threshold (> 2 MeV/n), REL rate for ions are calculated as $S(E, T_{cut}) = z_i^2 S_p(E_s, T_{cut}) + F(E, z_i) + G(E)$

where G is a correction term

Stopping power algorithm

Contd.

Stopping power S_p based on restricted energy loss (Bethe formula) and is given by:

$$S_p = 2\pi r_e^2 m_e c^2 \times \frac{n_{el}}{\beta^2} \left[\ln \left(\frac{2m_e c^2 \beta^2 T_{cut}}{(1 - \beta^2) I^2} \right) - \beta^2 \left(1 + \frac{T_{cut}}{T_{max}} \right) - \delta - 2 \frac{C}{Z_2} \right]$$

where

n_{el} is electron density of the material

I is mean excitation energy

Scaled energy is calculated as

$$E_s = EM_p / M_{ion}$$

where M_p = mass of proton

M_{ion} = mass of ion

Ionisation

The ionization process is included in Electromagnetic Physics model as **G4ionIonisation class**. This class provides the continuous energy loss due to ionization. This consists of further three **classes**.

G4BetheBlochModel ($T > 2 \text{ MeV}$)

G4BraggModel ($T < 2 \text{ MeV}$)

G4BraggIonModel ($T < 2 \text{ MeV}$)

Continuous energy loss is calculated by Bethe Bloch relation

Binary Cascade Model

Binary Cascade model (*G4BinaryLightIonReaction*) is used to describe the **nucleon-nucleon collisions**. The production of secondary particles has also taken into consideration.

Binary Cascade Model

- In this model, interaction between primary and secondary particle with *individual nucleon and nuclei* is considered.
- Available *cross section classes (theoretical models)* activated for the simulation
- The cascade terminates when the average energy of *secondary particles is below threshold.*
- The *number of particles* produced from the cascade is given roughly by

$$N_m = C(s)[A^{1/3} - 1]N_{ic}$$

where A is the Atomic mass

C(s) is function of s, square of centre of mass energy

N_{ic} is the number of hadrons generated in the initial collision

Binary Cascade Model

- For heavy nuclei with $A > 16$,
Nuclear density is

$$\rho(r_i) = \rho_0 / [1 + \exp\{(r_i - R)/a\}]$$

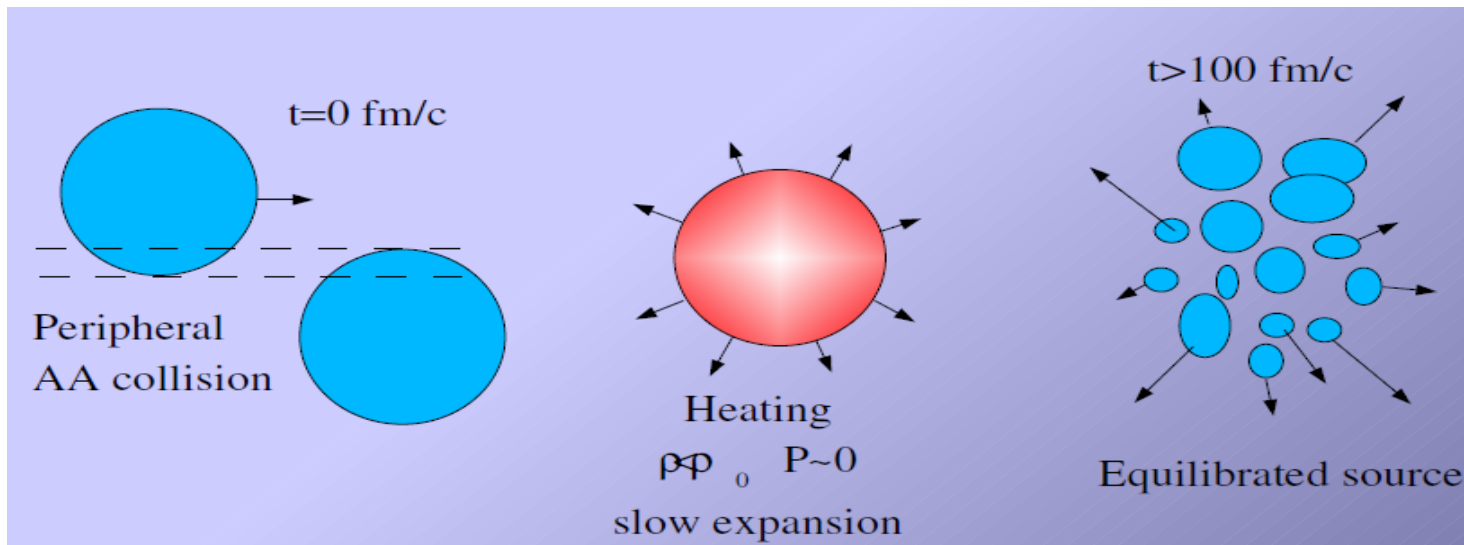
$$\text{where } \rho_0 \approx \frac{3}{4\pi R^3} \left(1 + \frac{a^2 \pi^2}{R^2}\right)^{-1}$$

$$R = r_0 A^{1/3} \text{ fm and } r_0 = 1.16 (1 - 1.16A^{-2/3})$$

$$a \approx 0.545$$

Statistical Multifragmentation model

The statistical multifragmentation model is included in Geant4 as ***G4StatMF***. This model is used to describe the multifragment breakup of excited nuclei.



- The G4StatMF is capable to predict *final states* as a result of highly excited nucleus *breakup*.
- This model is applied for excitation energy per nucleon $(U/A) > 3 \text{ MeV}$ (set in code, manually).
- The excited fragments propagate *independently and undergo de-excitation*.

Statistical Multifragmentation model

It is based on the probability of Multifragmentation.
The probability of a breakup channel is:

$$W_b(U, A, Z) = \frac{1}{\sum_b \exp[S_b(U, A, Z)]} \exp[S_b(U, A, Z)]$$

where $S_b(U, A, Z)$ is the entropy of multifragment state

Constraints are $\sum_f \langle N_{A_f, Z_f} \rangle A_f = A$

and $\sum_f \langle N_{A_f, Z_f} \rangle Z_f = Z$

Probability distribution is given by Gaussian as

$$P(Z_f(A_f)) \sim \exp \left[-\frac{(Z_f(A_f) - \langle Z_f(A_f) \rangle)^2}{2(\sigma_{Z_f}(A_f))^2} \right]$$

Charge and atomic number distribution

According to Poisson distribution, fragment with atomic numbers $A_f > 1$ is given by:

$$\langle N_{A_f} \rangle = A_f^{3/2} \frac{V_f}{\lambda_{T_b}^3} \exp \left[\frac{1}{T_b} (F_f(T_b, V) - F_f^t(T_f, V) - \mu A_f - \nu \langle Z_f \rangle) \right],$$

The average charge Z_f for the fragment having atomic number A_f is given by

$$\langle Z_f(A_f) \rangle = \frac{(4\gamma + \nu)A_f}{8\gamma + 2[1 - (1 + \kappa)^{-1/3}]A_f^{2/3}}$$

Kinetic energy distribution of fragments

Kinetic energy according to Boltzmann distribution of fragments is given by:

$$\frac{dP(T_{kin}^f)}{dT_{kin}^f} \sim \sqrt{T_{kin}^f} \exp(-T_{kin}^f/T_b)$$

where T_{kin}^f is the rest kinetic energy of fragment

And excitation energy of the fragments is:

$$U_f(T_b) = E_f(T_b) - E_f(0) = \frac{T_b^2}{\epsilon_0} A_f + [\beta(T_b) - T_b \frac{d\beta(T_b)}{dT_b} - \beta_0] A_f^{2/3}$$

Fermi breakup model

Fermi Break up is included in Geant4 as ***G4FermiBreakUp***. This breakup model is used to describe highly excited light nuclei for the fragments with **$A \leq 16$** and **$Z \leq 8$** .

Breakup Probability

The total probability of a nucleus to break up into n components (*nucleons, deuterons, triton, alphas etc.*) is given by

$$W(E,n) = (V/\Omega)^{n-1} \rho_n(E)$$

where $\rho_n(E)$ is the density of a number of final states

V is the volume of the system

And $\Omega = h^3$, is the normalization factor

The total kinetic energy E_{kin} of all the fragments is given by:

$$E_{kin} = U + M(A, Z) - E_{Coulomb} - \sum_{b=1}^n (m_b + \epsilon_b)$$

Breakup Probability

Coulomb barrier for a given channel is given by

$$E_{Coulomb} = \frac{3e^2}{5r_0} \left(1 + \frac{V}{V_0}\right)^{-1/3} \left(\frac{Z^2}{A^{1/3}} - \sum_{b=1}^n \frac{Z^2}{A_b^{1/3}} \right)$$

where V_0 is the system corresponding to the normal nuclear matter density and $\kappa = V/V_0$ (generally, $\kappa = 0$).

The total probability for nucleus to break-up into n components in the final state is given by

$$W(E, n) = (V/\Omega)^{n-1} \rho_n(E)$$

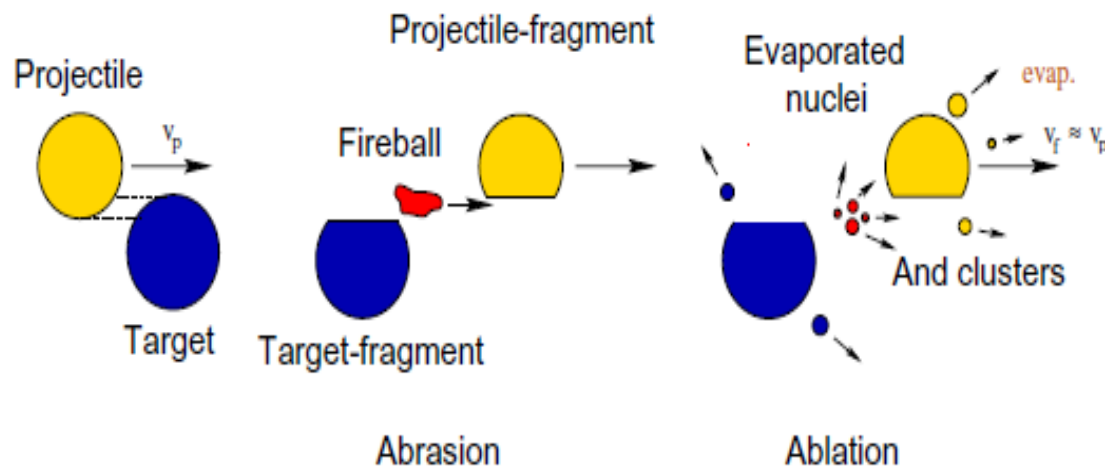
where $\rho_n(E)$ is the density of final states

V is the volume of decaying system

$\Omega = h^3$ is the normalization volume

Abrasion-ablation model

- At energies greater than 100 MeV/n, peripheral collisions are the most frequently occurring nuclear reactions.
- These reactions result in fragmentation of both target as well as projectile nuclei and explained by two-step abrasion-ablation model.



Quantum molecular dynamics (QMD) model

- Interaction of particles with matter undergoes both dynamics and statistical effects.
- In QMD model, dynamics considerations are taken into account to study the nuclear interactions and simulate the quantum effects.
- The particle-particle correlations are studied by considering individual collisions.

The equation of the particle is defined by:

$$\psi_i(\vec{r}, t) = \frac{1}{(2\pi L)^{3/4}} \exp \left[-\frac{(\vec{r} - \langle \vec{r}_i(t) \rangle)^2}{4L} + \frac{i}{\hbar} \langle \vec{p}_i(t) \rangle \vec{r} \right]$$

Applications of Geant4

- Medical applications where interactions of radiations used for treatment (hadrontherapy) are simulated.
- Space applications where it is used to study interactions between the natural space radiation environment and space hardware or astronauts and for shielding design.
- Radiation effects in microelectronics where ionizing effects on semiconductor devices are modeled.
- Nuclear physics

Features

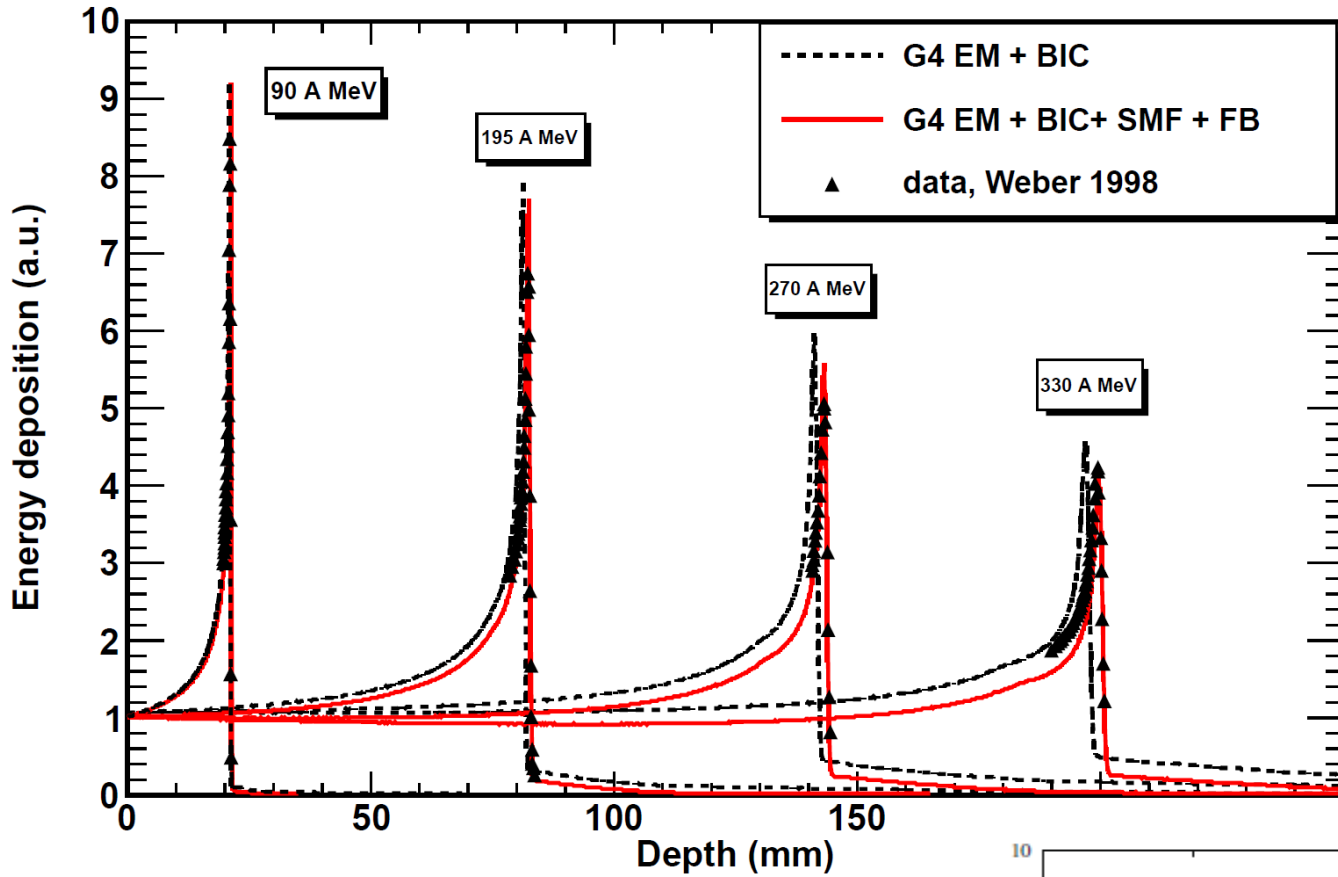
- geometry
- tracking
- detector response
- run management
- visualization and
- user interface.

For many physics simulations, it required less time to be spent on the low level details, and researchers can start immediately on the more important aspects of the simulation.

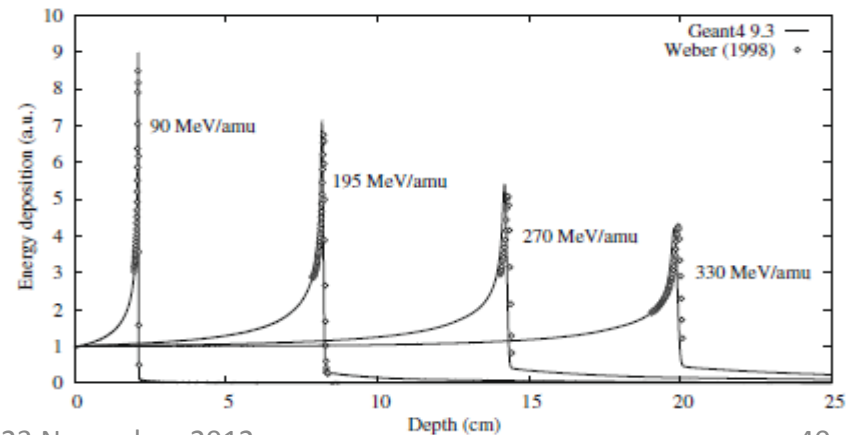
- The application give the possibility to simulate a typical hadrontherapy treatment beam line (including all its elements) and to calculate the proton/ion dose distribution curves.
- It calculates the depth dose distribution in a given material: to do this a cylinder divided in slices is simulated and the energy deposited in each slice is collected. This permit the simulation of a typical, plane parallel, ionization chamber used in the hadrontherapy practice.
- Lateral dose distributions can be obtained; the user can choose the phantom materials, the beam mean energy and the angle of the modulator wheel; the user can visualize the experimental set-up.

Results published by our group:
 ^{12}C ions in polyethylene medium

Kumar et al., *Adv. Space Res.*, 49 (2012) 604.

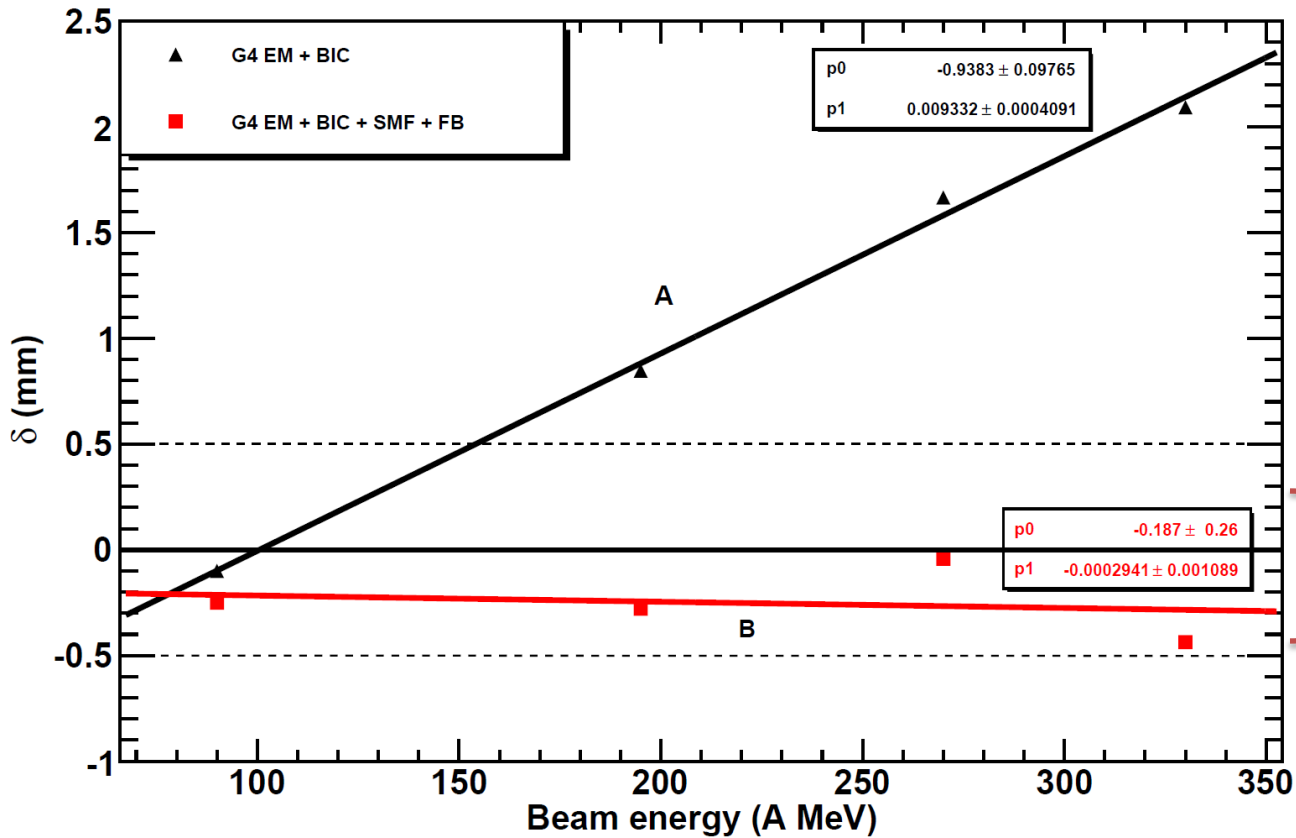


Lechner et al., *Nucl. Instrum. Meth. B*, 268 (2010) 2343.



From G4QMDReaction model

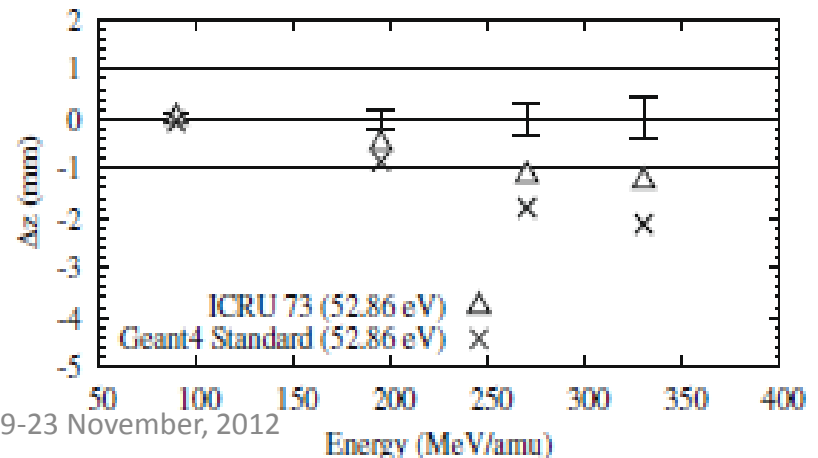
Deviation from the experimental results



Kumar et al., *Adv. Space Res.*, 49 (2012) 604.

Less than 0.5 mm

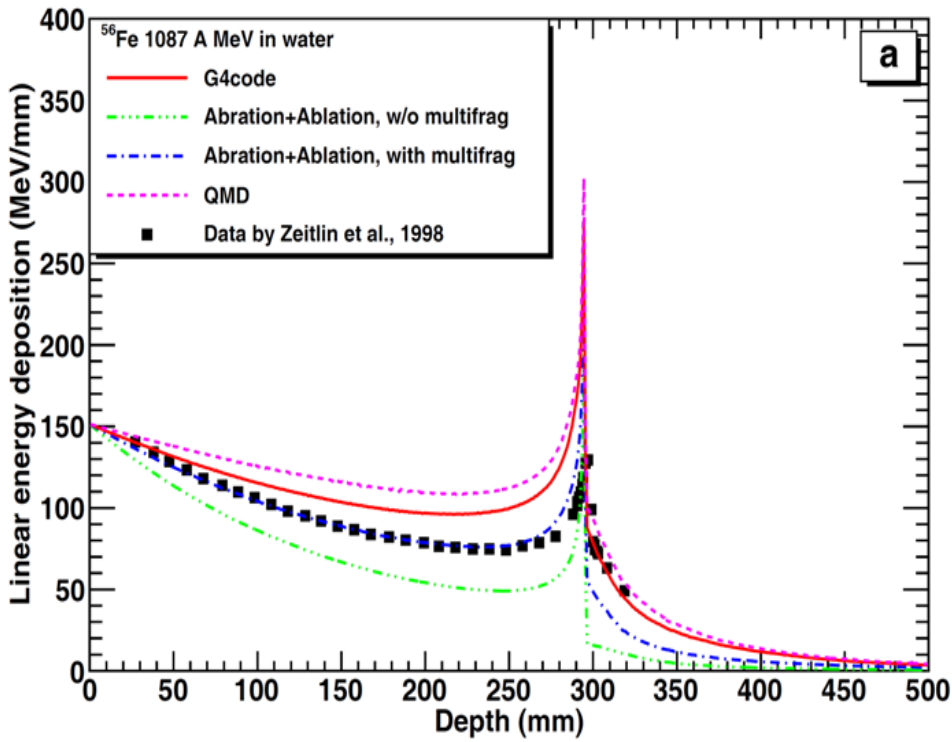
Lechner et al., *Nucl. Instrum. Meth. B*, 268 (2010) 2343.



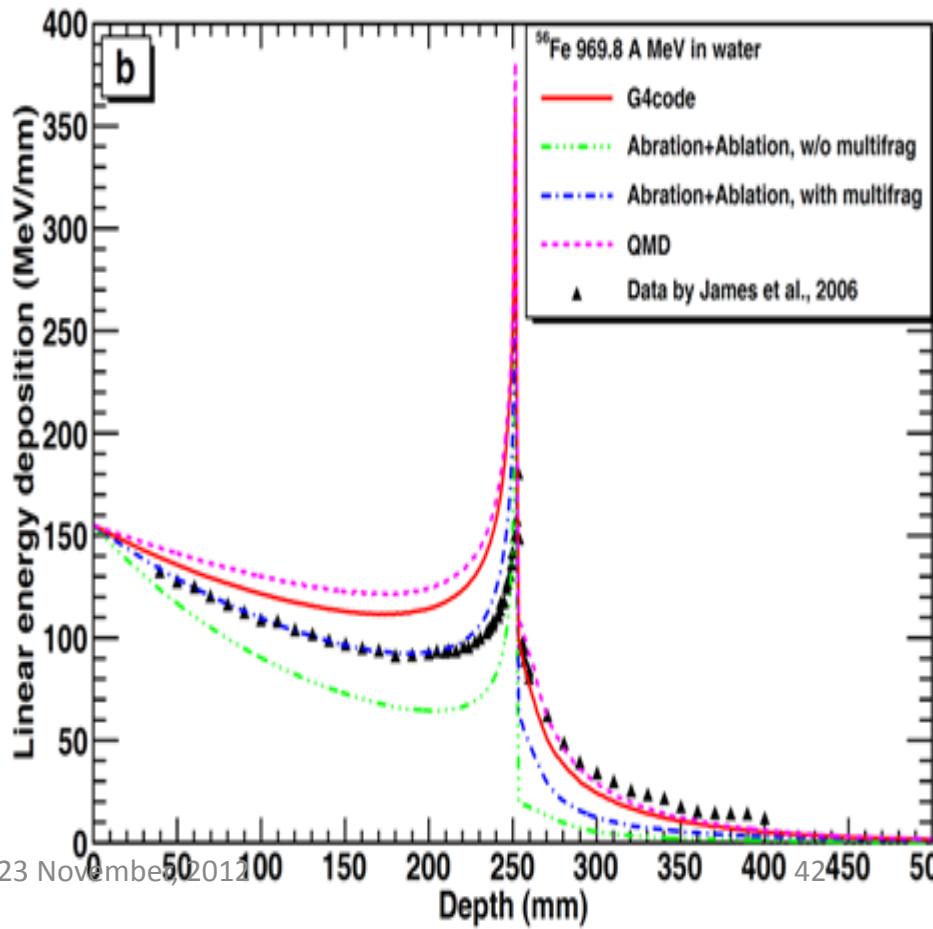
Dose-profile of 1087 and 969.8 A MeV ^{56}Fe in water

Jalota et al., *Nucl. Instrum. Meth. B*, 291 (2012) 7.

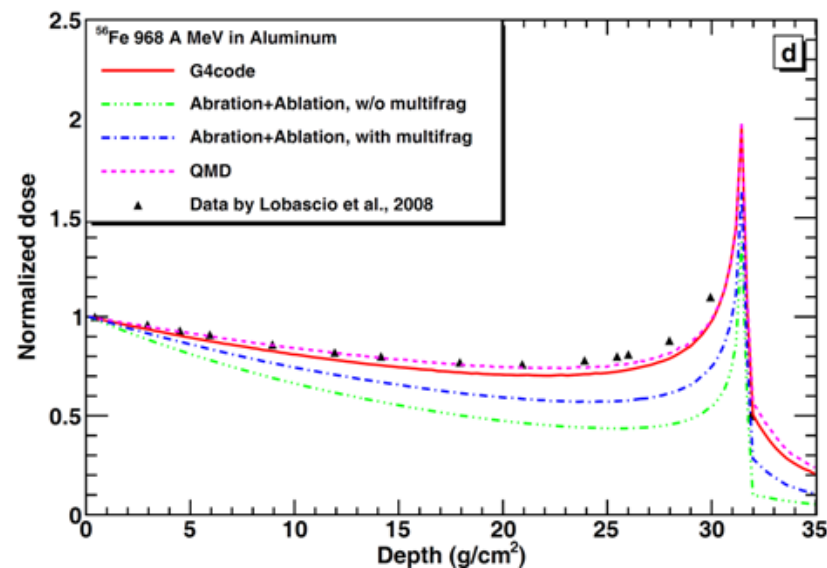
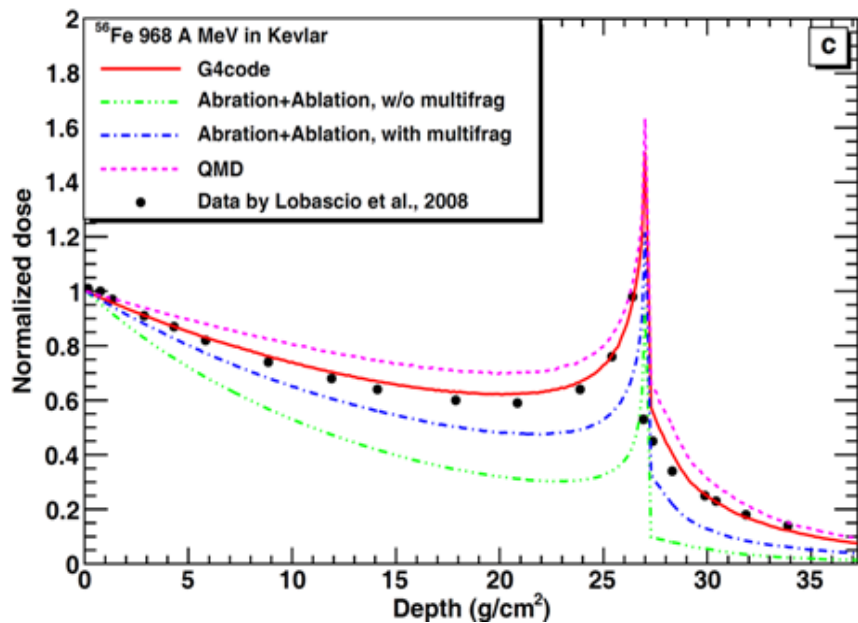
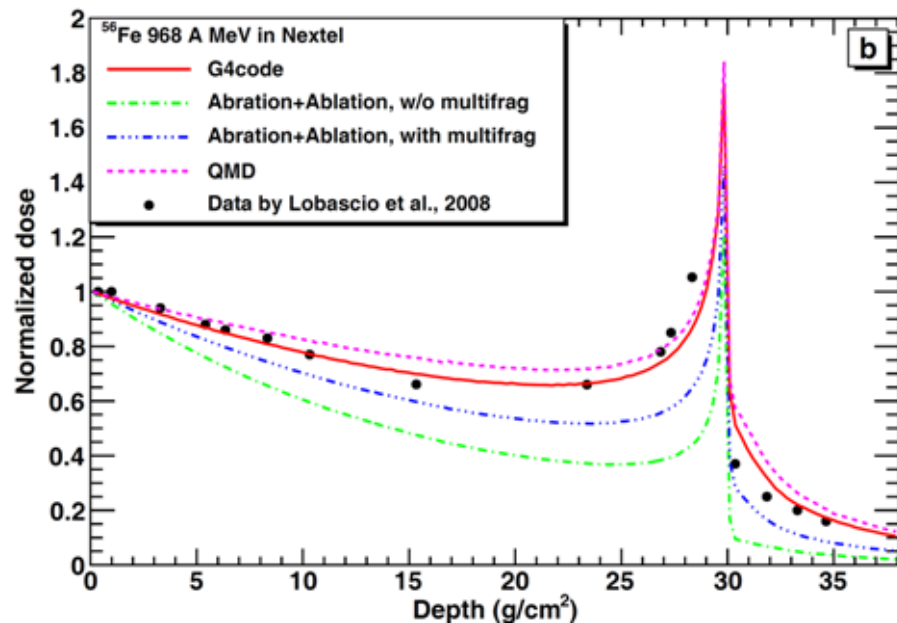
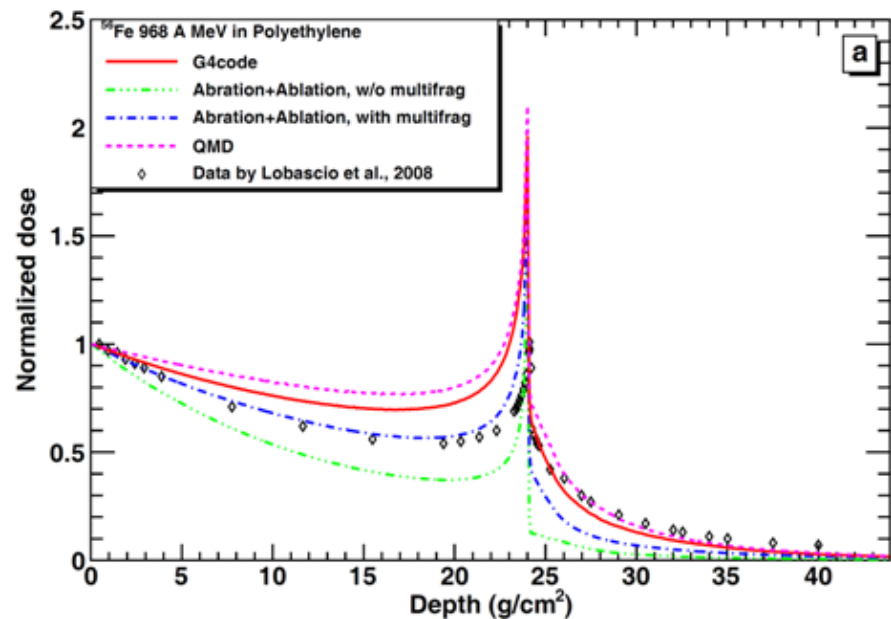
Data from M.R. James et al, *Nucl. Instrum. Meth. A*, 562 (2006) 819.



Data from C. Zetilin et al. ,*Radiat. Res.*, 149 (1998) 560.



Dose-profile of 968 A MeV ^{56}Fe in polyethylene, Nextel, Kevlar and aluminum



Jalota et al., *Nucl. Instrum. Meth. B*, 291 (2012) 7.

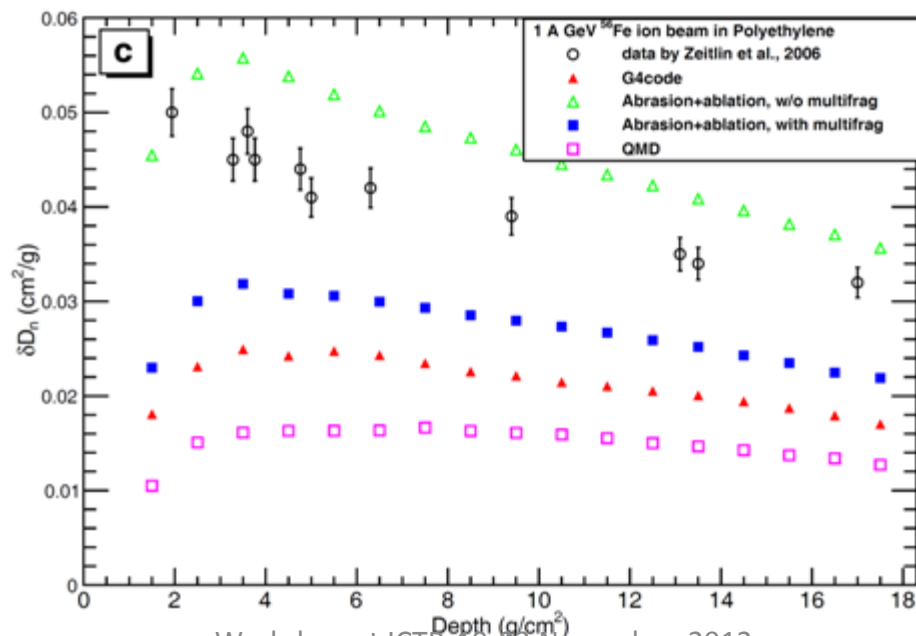
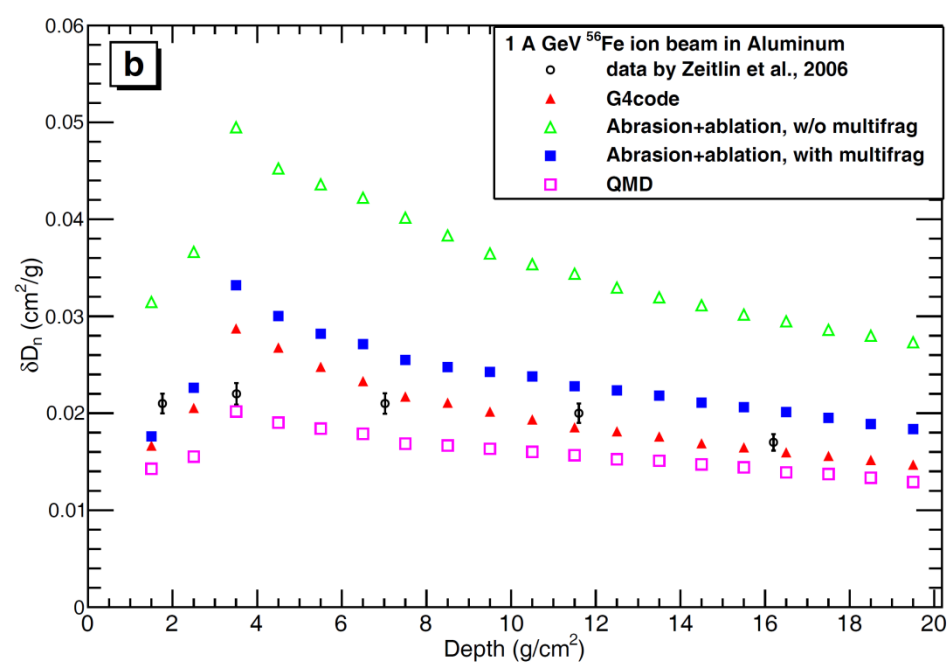
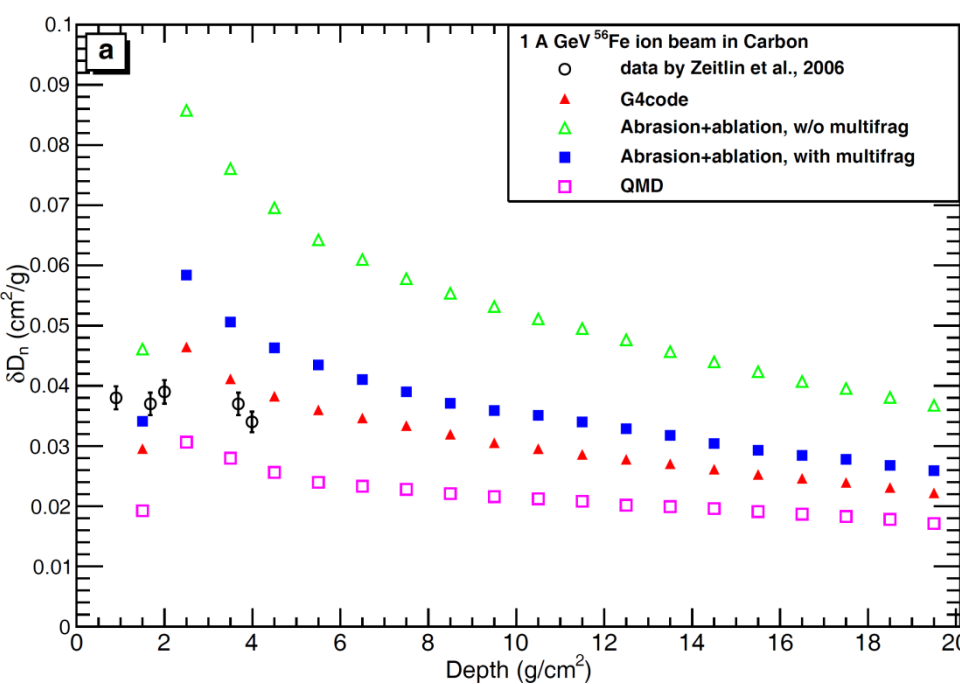
Dose-reduction

Dose-reduction is a parameter that is used to study the effectiveness of the shielding material.

Dose reduction per unit areal density δD_n (cm^2/g) is calculated as:

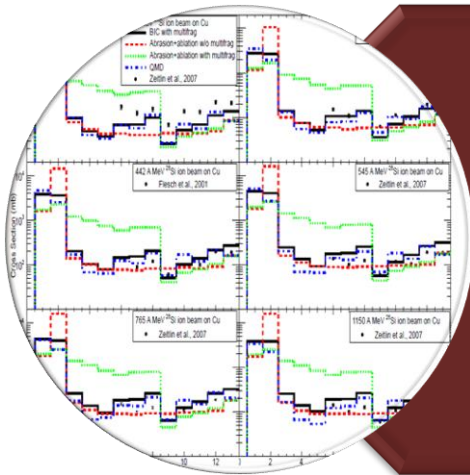
$$\delta D_n = \frac{1 - \frac{\text{dose}_i}{\text{dose}_1}}{\text{depth}_i}$$

where dose_i is calculated at the depth_i and dose_1 is the dose calculated at initial position



Jalota et al., *Nucl. Instrum. Meth. B*, 291 (2012) 7.

Data from C. Zeitlin et al., *Nucl. Instrum. Meth. B*, 252 (2006) 308.



Calculation of fragmentation production cross sections using **BIC**, **Abrasion-ablation** and **QMD** models

Fragmentation production cross sections

- Several experimental studies have been performed to calculate the fragmentation production cross section for various ions at different energies on several materials. e.g. Zeitlin et al. (NIM A, 2007), Webber et al. (Phy. Rev. C, 1990), Flesch et al. (Rad. Meas., 2001), Checcini et al. (Nuclear Physics A 807, 206-213, 2008) etc.
- Only few **simulation/theoretical studies** has been performed to calculate total fragmentation cross section. e.g Sihver (Adv. Space Res., 2012).
- As best to our knowledge, no simulation study has been performed yet for calculating **fragmentation production cross section**. (Present results to be submitted).

Fragmentation production cross section

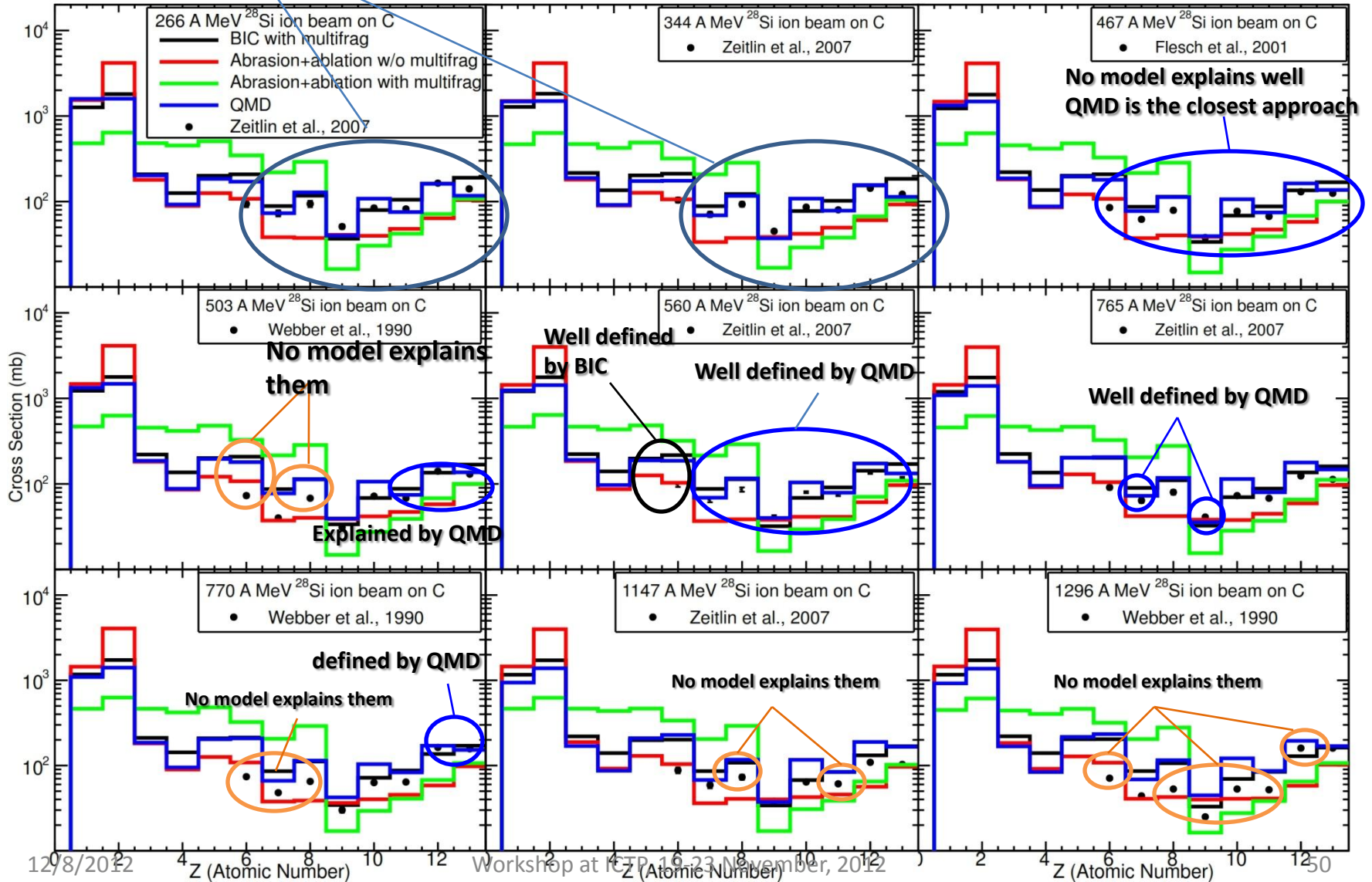
Nucleon-nucleon collisions are treated **classically**, using BIC and AA model; and **quantum mechanically** using QMD model.

At very high energy (\sim GeV/n), there is **small transverse in momentum**.

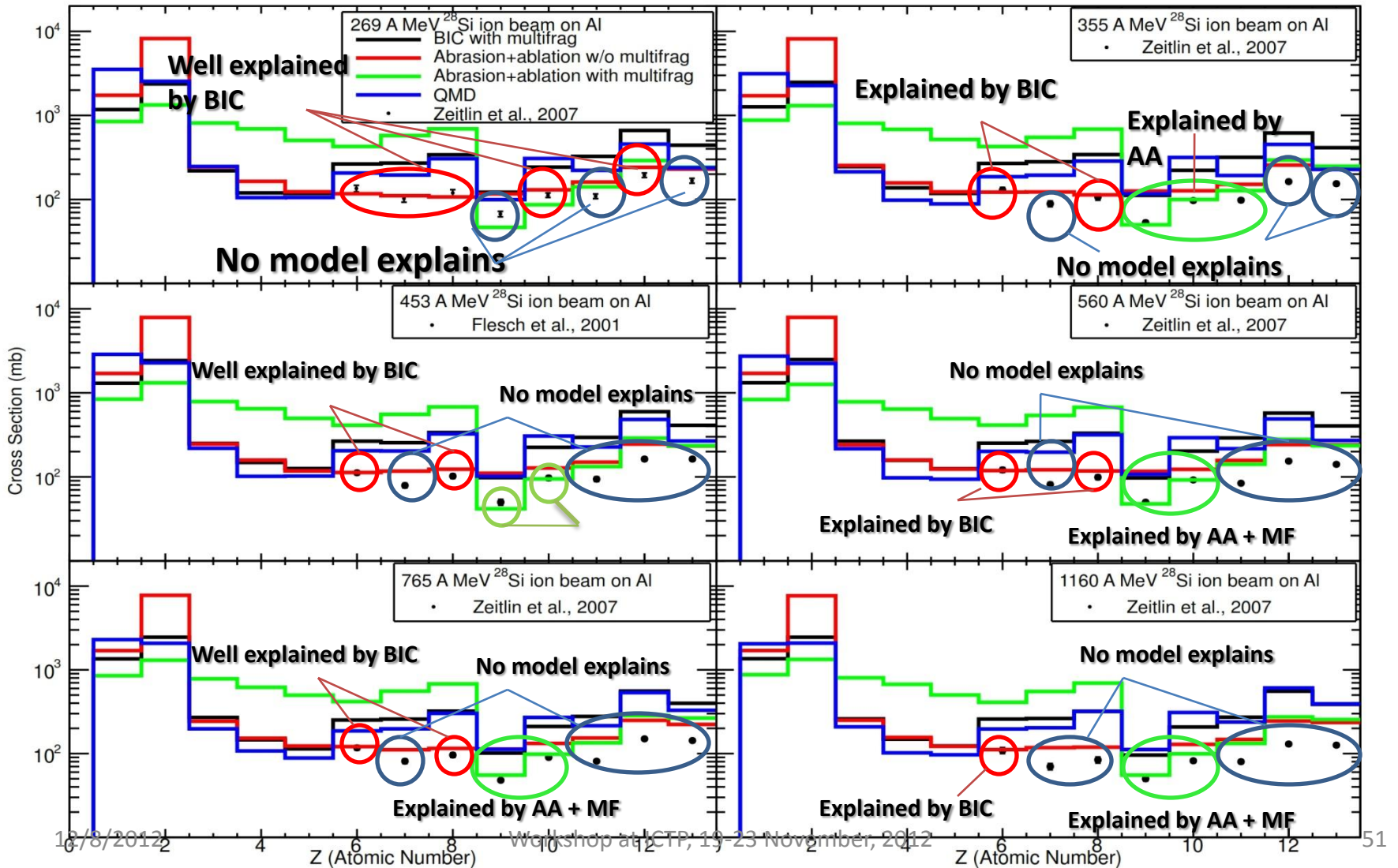
Fragments are collected/scored **at all angles**.

^{28}Si on C

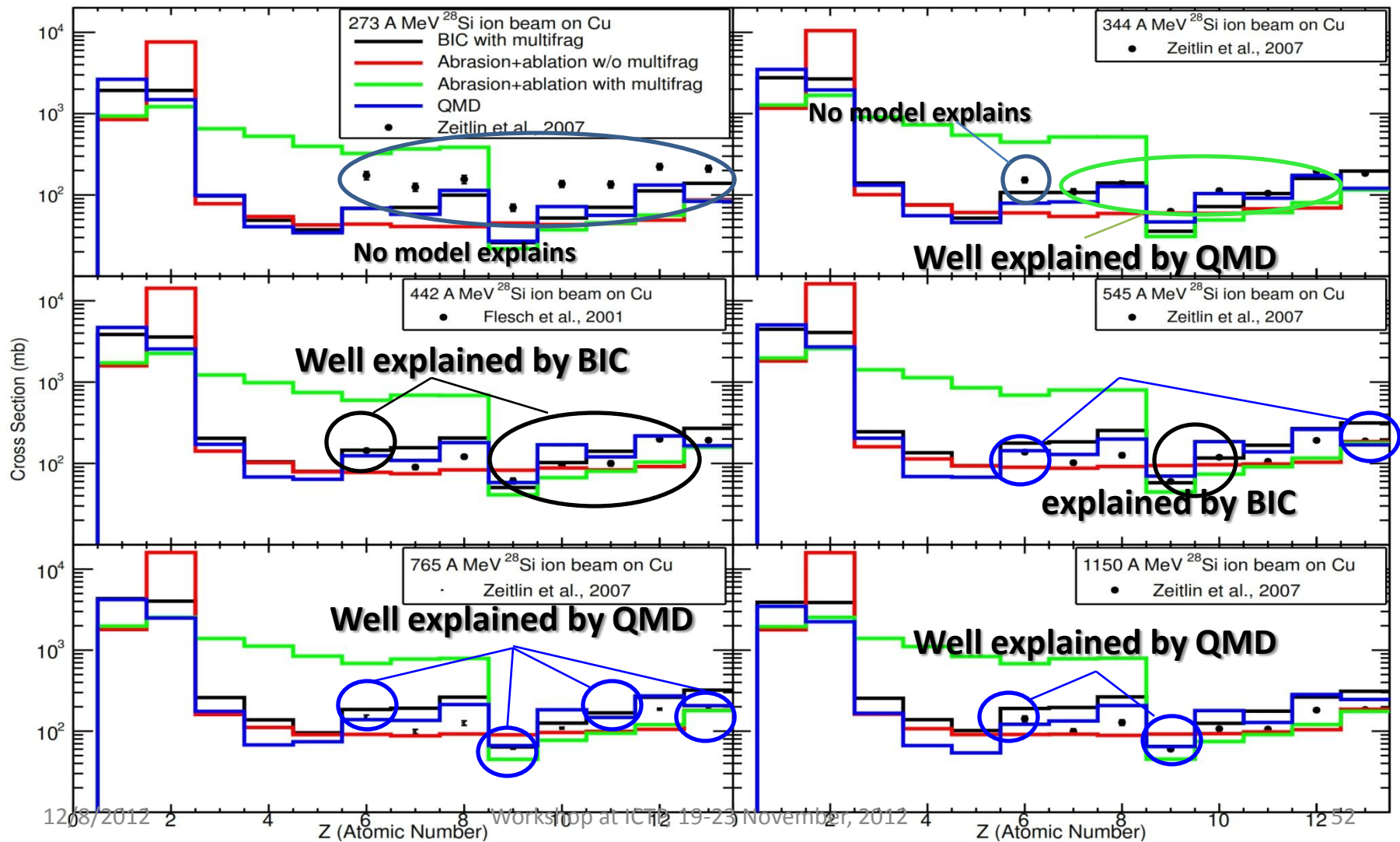
Well explained by QMD model



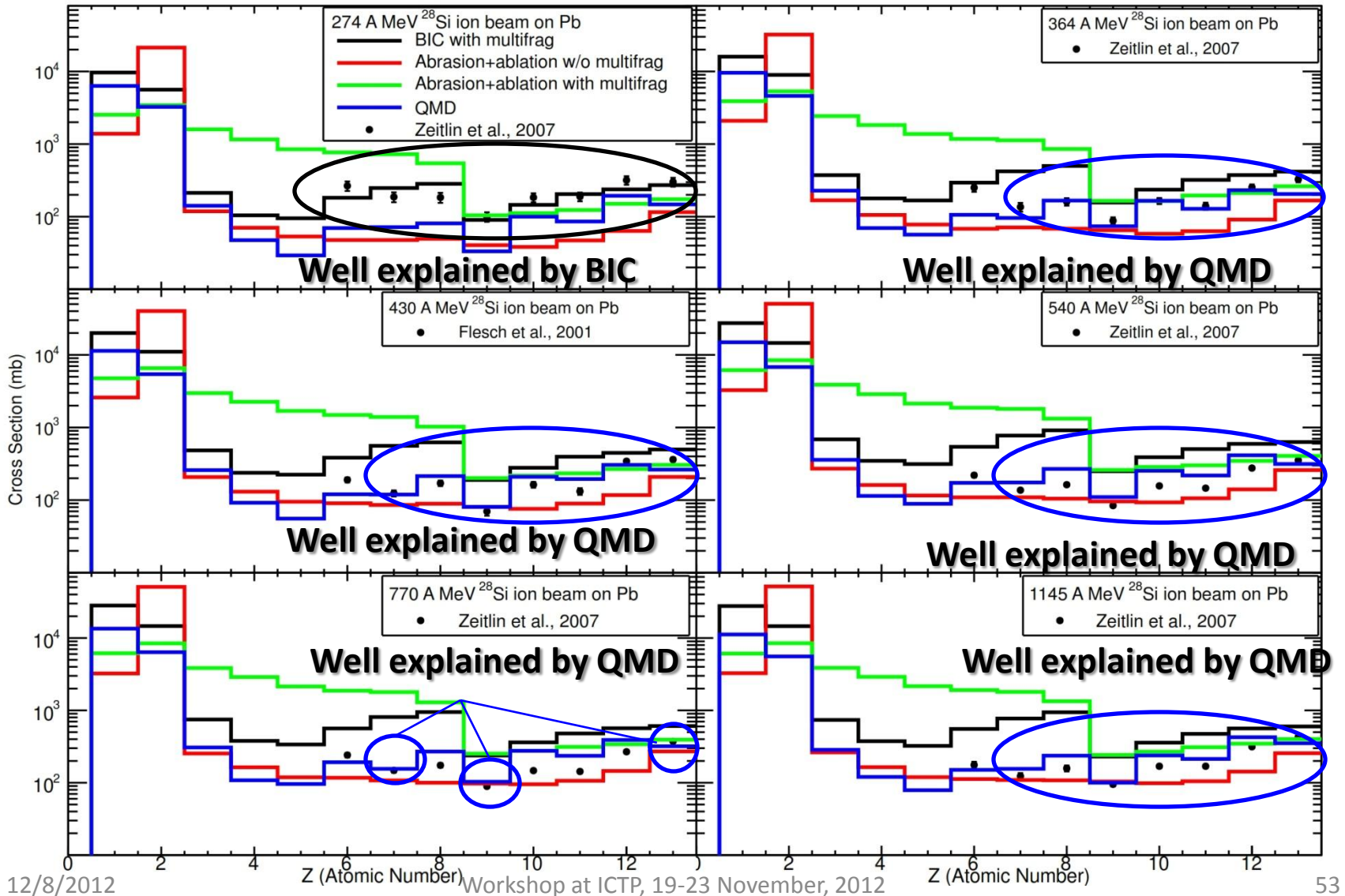
^{28}Si on Al



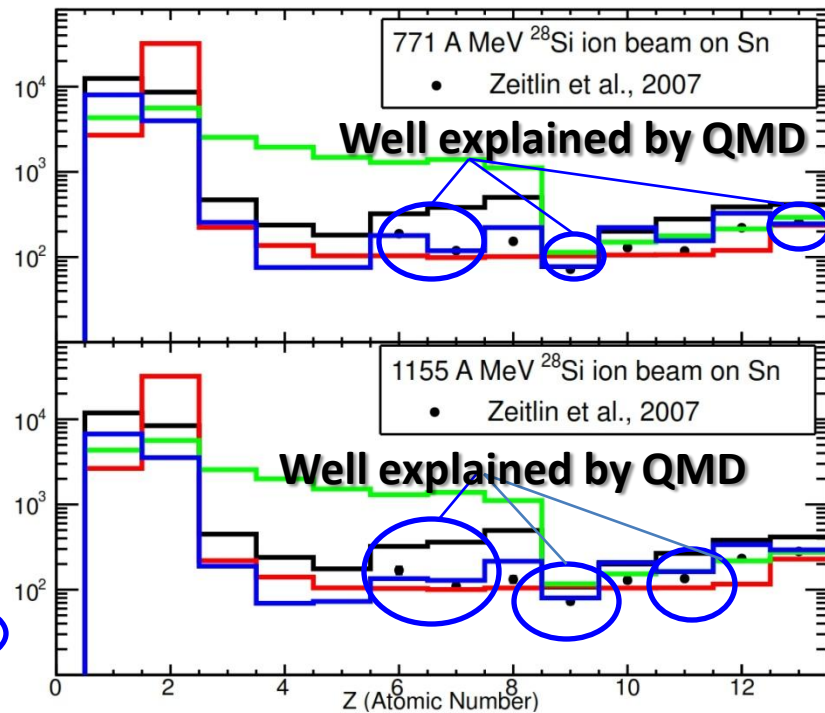
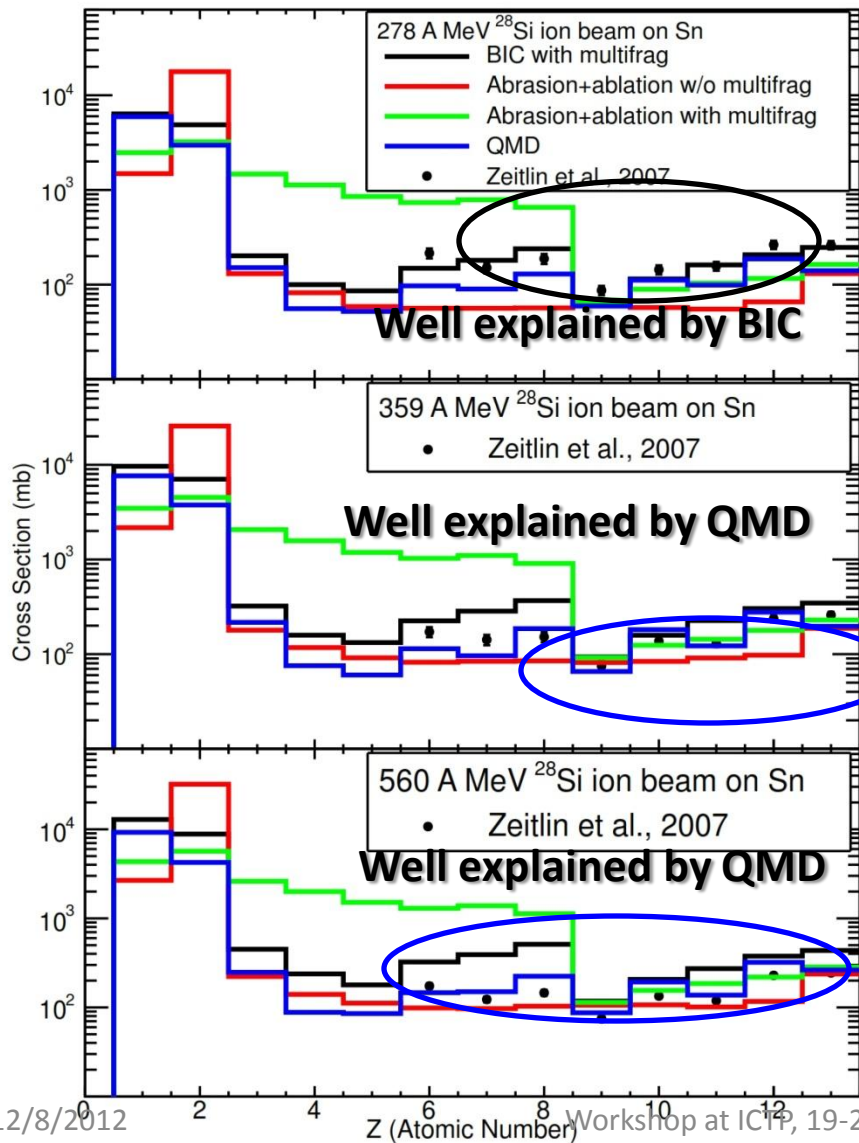
^{28}Si on Cu



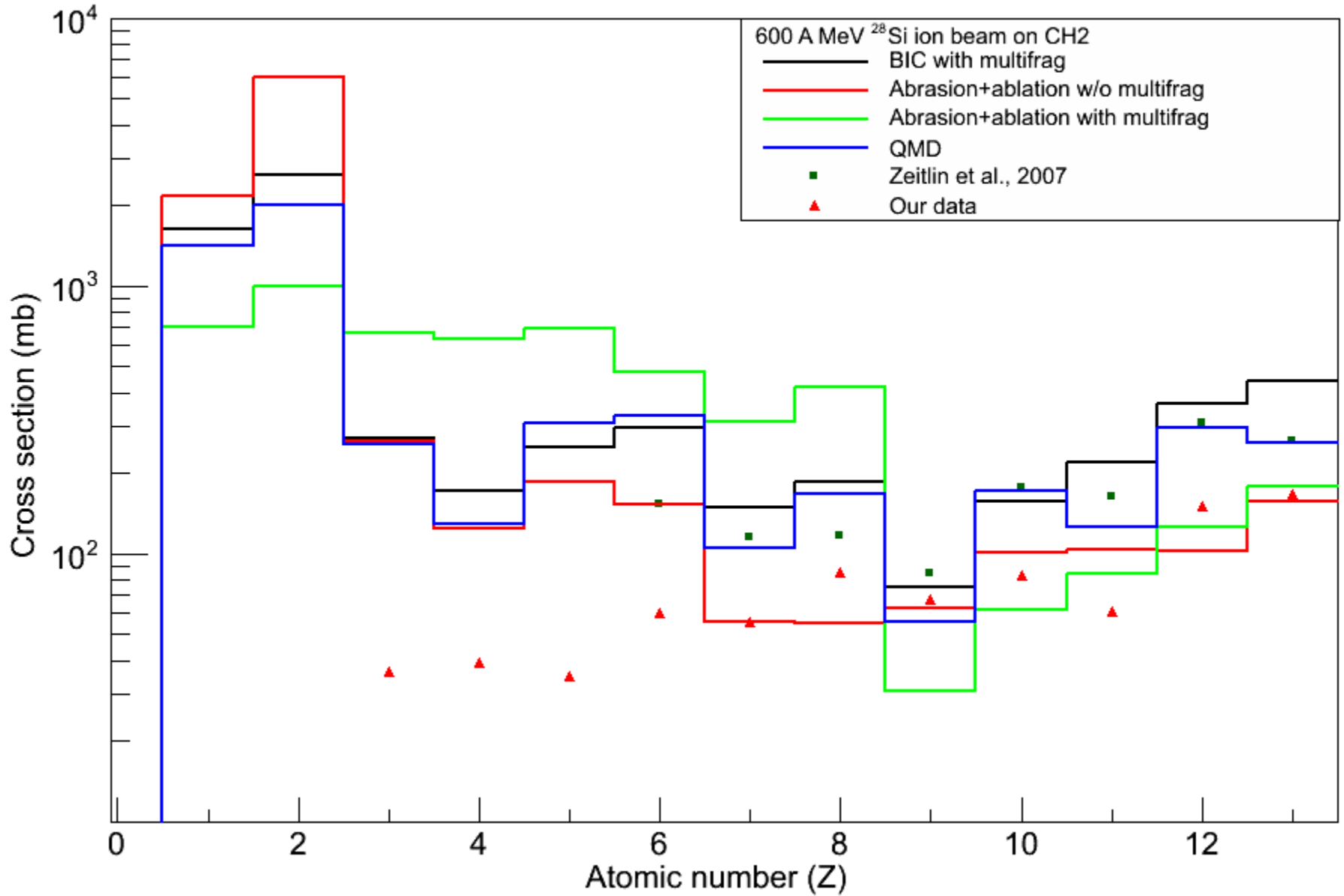
^{28}Si on Pb



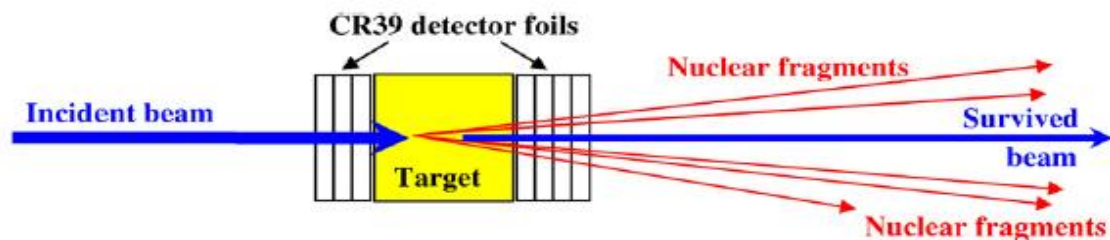
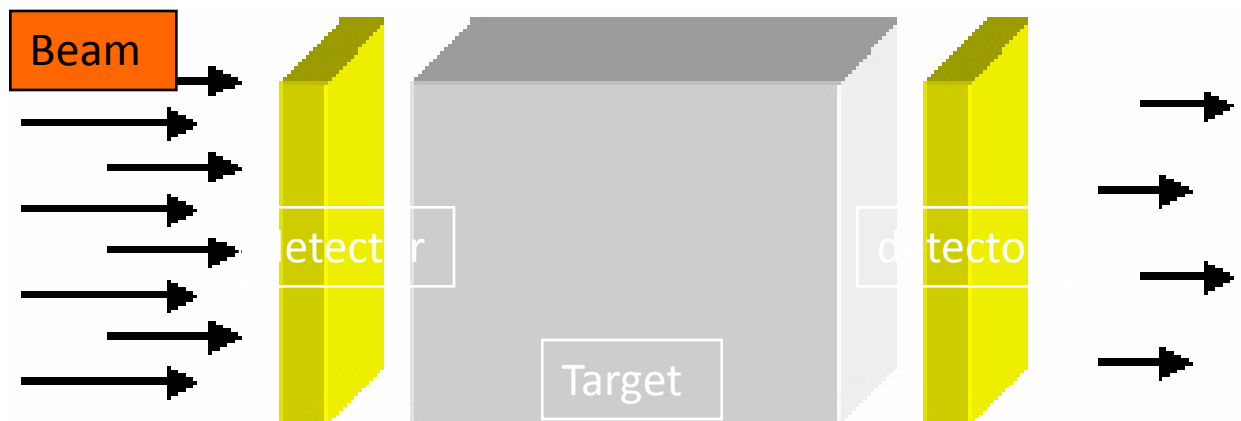
^{28}Si on Sn



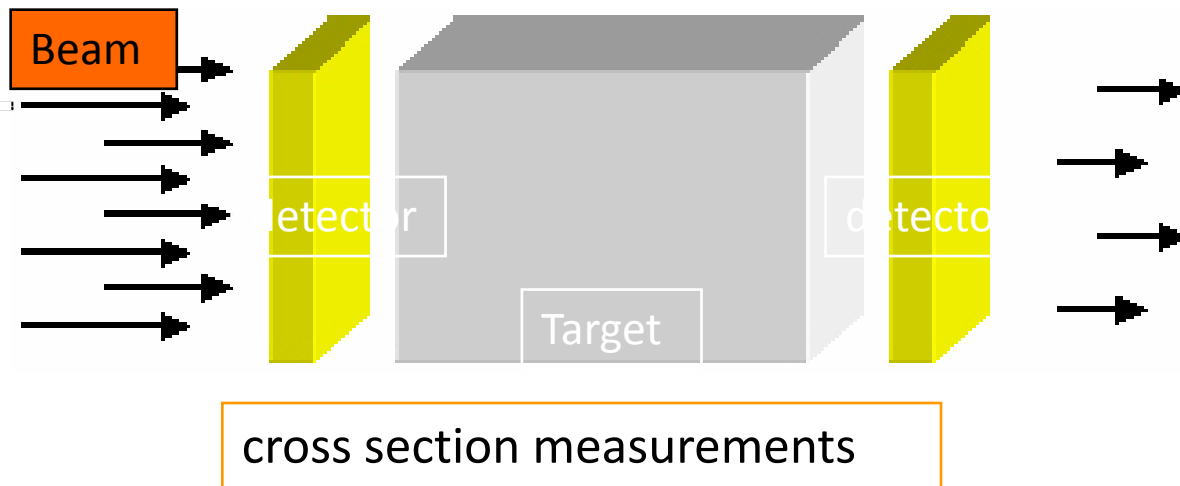
Preliminary results: (Thick target)



Experimental work using NTDs



The target thicknesses will be chosen to be sufficiently large to give good fragment statistics, but thin to keep the corrections for secondary nuclear interactions in the target reasonably small.



$$\sigma_{\text{tot}} = \frac{A_T \ln(N_{\text{in}}/N_{\text{out}})}{\rho t N_{\text{Av}}} \quad \sigma(Z_i, Z_f) \approx \frac{1}{Kt} \frac{N_f}{N_i}$$

$$\sigma_{\Delta Z} = \frac{1}{Kt} \left(\frac{N_{\text{out}}^f}{N_{\text{S}}^p} - \frac{N_{\text{in}}^f}{N_{\text{in}}^p} \right)$$

Etching bath



Etching bath

Outlet

Thermostat

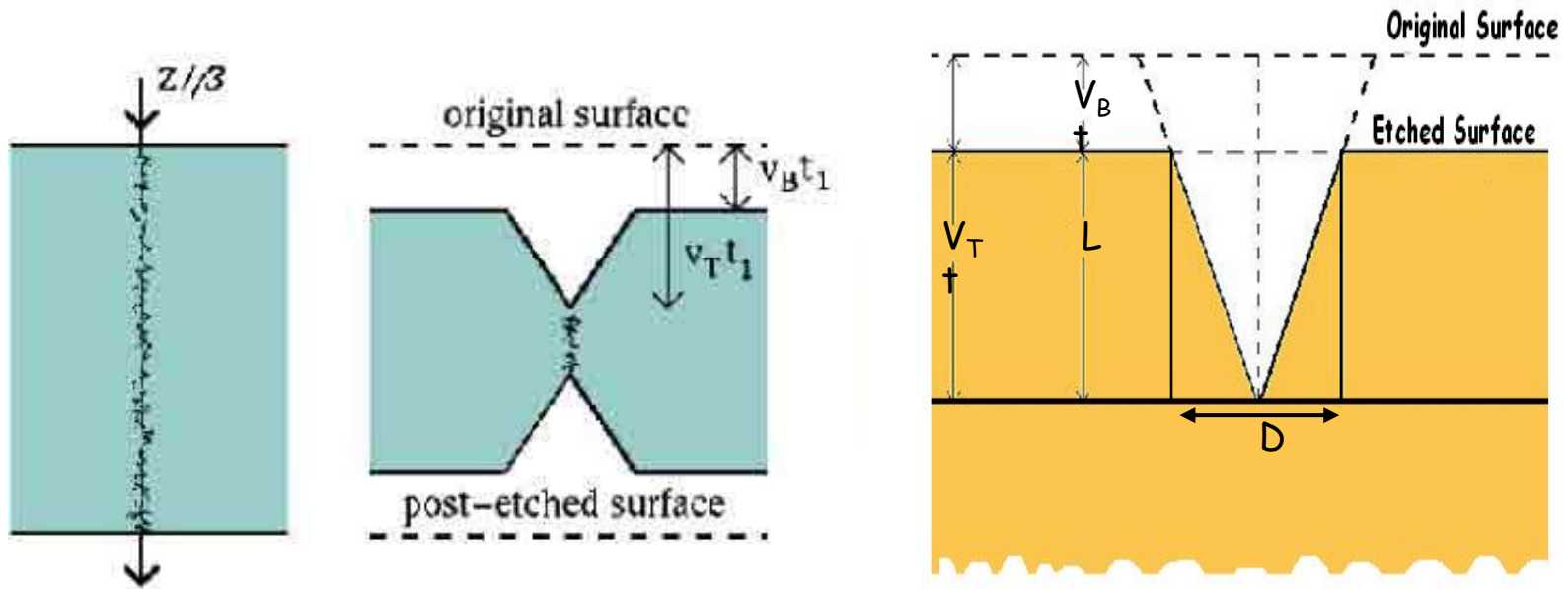


Control-panel

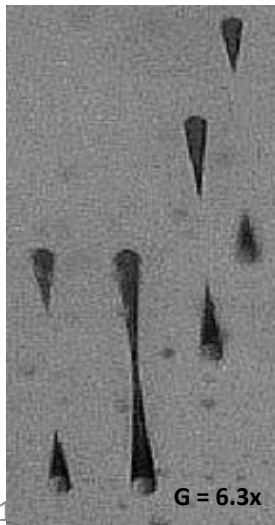
Stirring system

The chemical etching was performed in etching bath in 6 N NaOH solution + 1% ethyl alcohol at 70 °C for 95 hours in two steps.

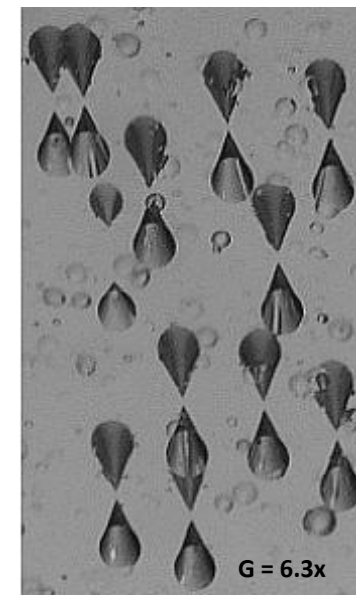
TRACK SHAPE PARAMETERS



158 AGeV Pb⁸²⁺



0.414 AGeV Fe²⁶⁺



Track diameter:

$$D = 2v_B t \left[\frac{(v_T - v_B)}{(v_T + v_B)} \right]^{1/2}$$

Track length:

$$L_e = (v_T - v_B) \cdot t$$

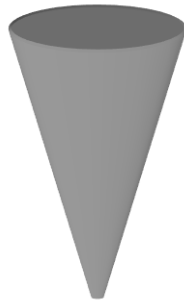
Reduced etch rate:

$$p = v_T / v_B$$

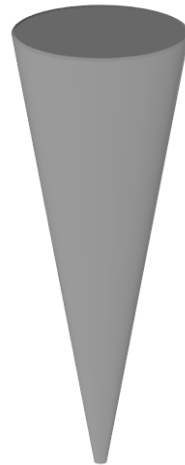
LENGTH AND BASE AREA OF TRACKS IN CR39 EXPOSED TO Pb^{82+} IONS (158 A GEV)



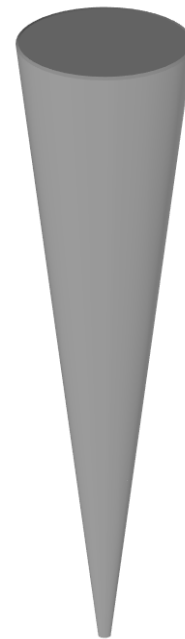
$Z = 20e$
 $D = 40 \mu m$
 $L = 23 \mu m$



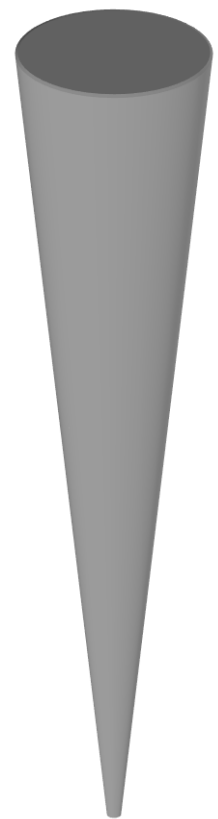
$Z = 45e$
 $D = 59 \mu m$
 $L = 77 \mu m$



$Z = 65e$
 $D = 69 \mu m$
 $L = 169 \mu m$



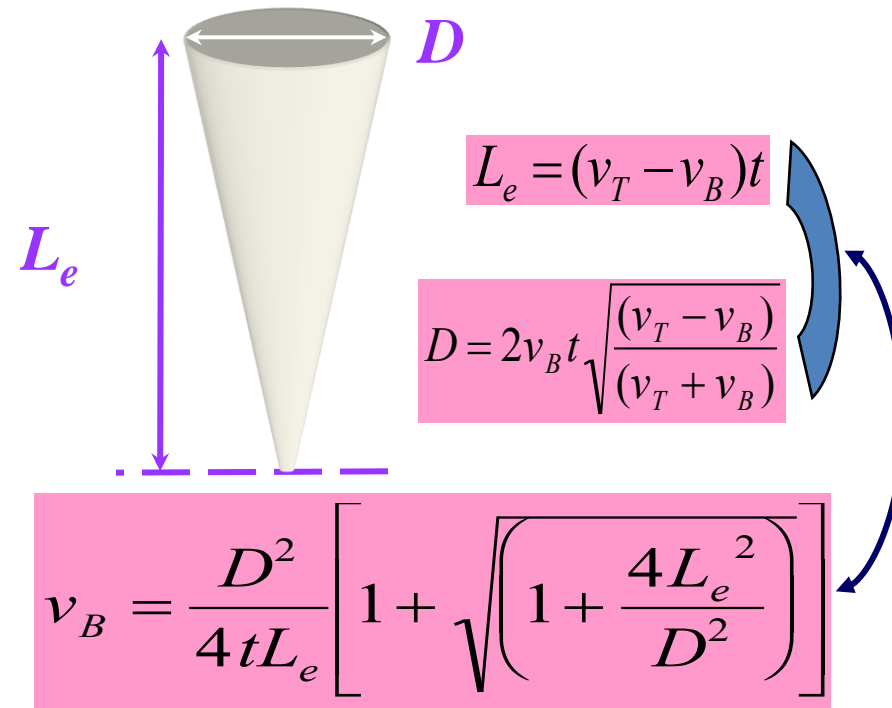
$Z = 76e$
 $D = 74 \mu m$
 $L = 425 \mu m$

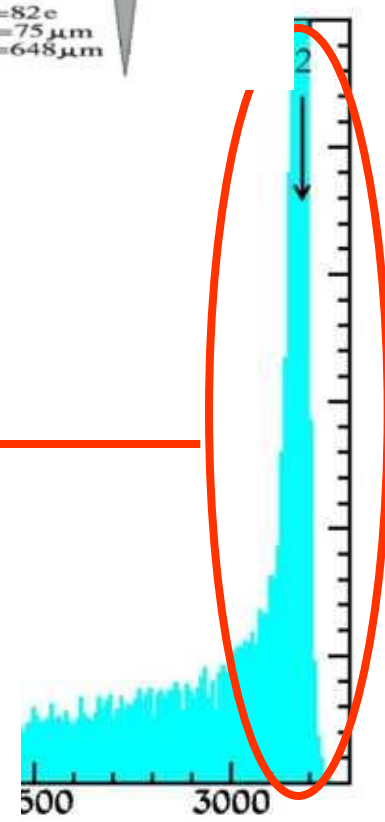
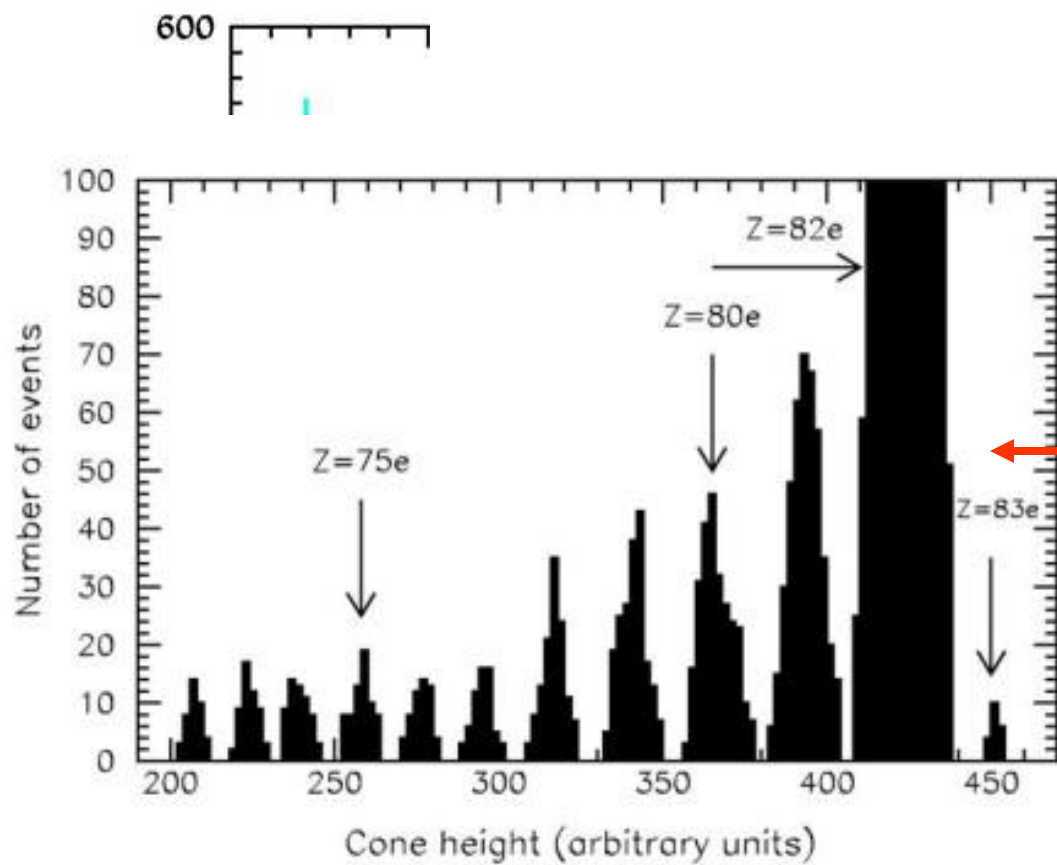
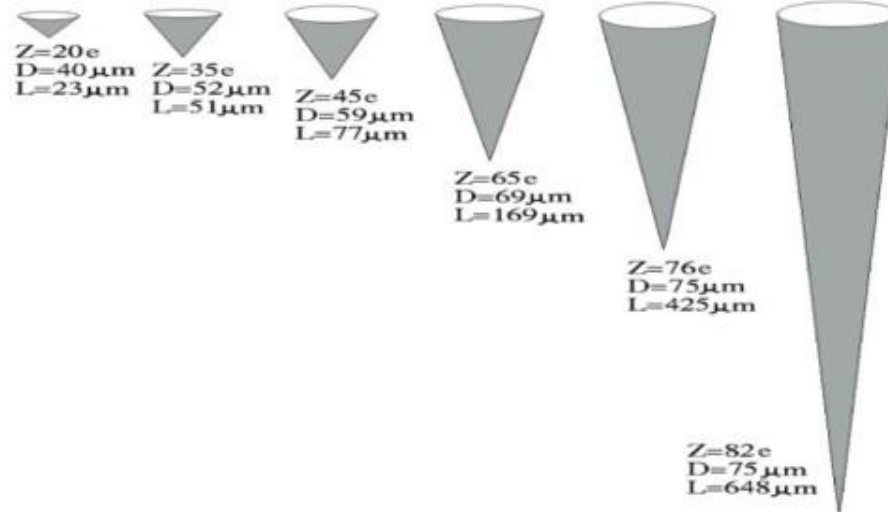


$Z = 82e$
 $D = 75 \mu m$
 $L = 650 \mu m$

BULK ETCH RATE (v_B) MEASUREMENTS

By D- L_e method





Automatic Image analyzer

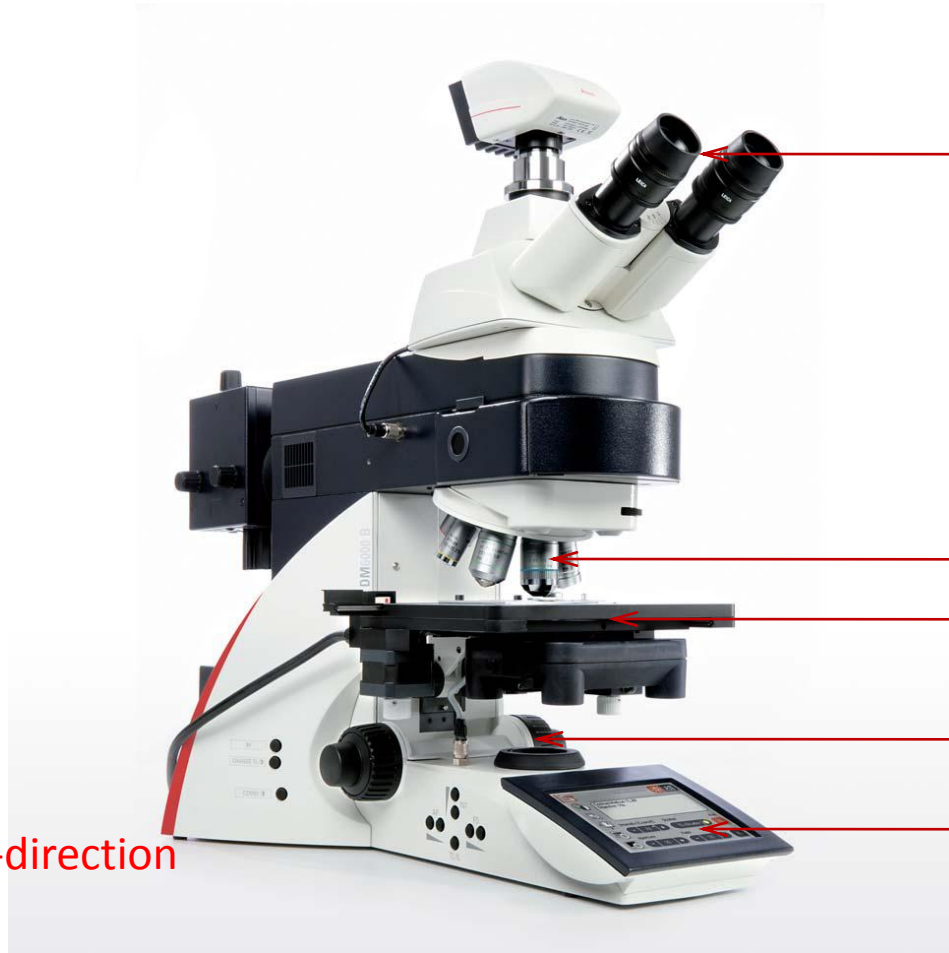
Move in x-direction

Focus



Move in y-direction

Leica SmartMove



Eye-piece

objectives

XY-stage

Focus drive

SmartTouch panel

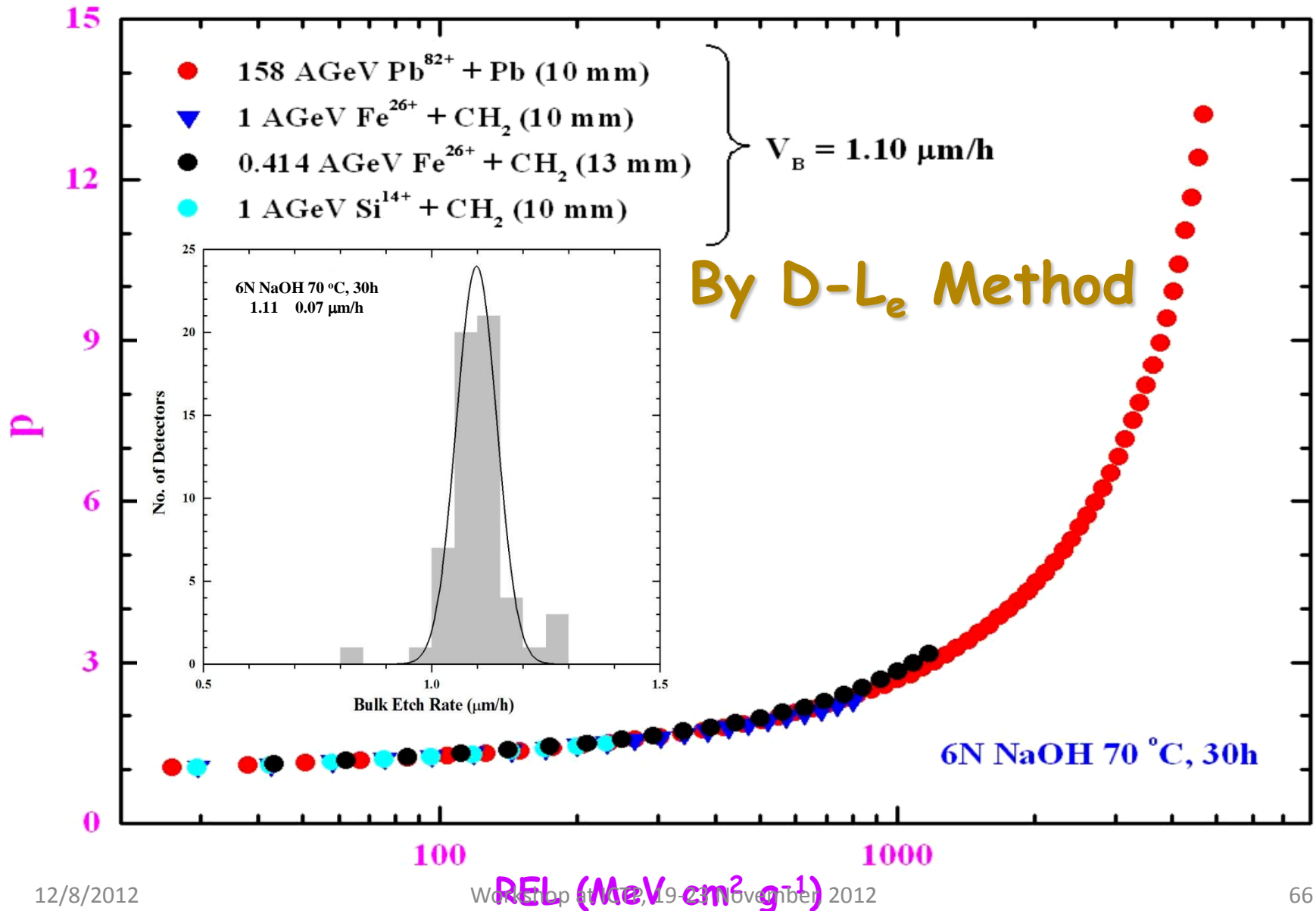
Features of Automatic Image Analyzer

- The microscope consists of a CCD camera, a frame grabber and a personal computer (PC) consisting of hardware and software interface. The microscope is equipped with a motorized X/Y stage with an accuracy of better than 1 μm .
- This stage can be controlled in dual ways; by using remote control element and by computer. By the remote control, movement of the stage along X-axis, along Y-axis, focus adjustment and some other functions can be performed.
- Leica SmartTouch displays the current microscope settings.

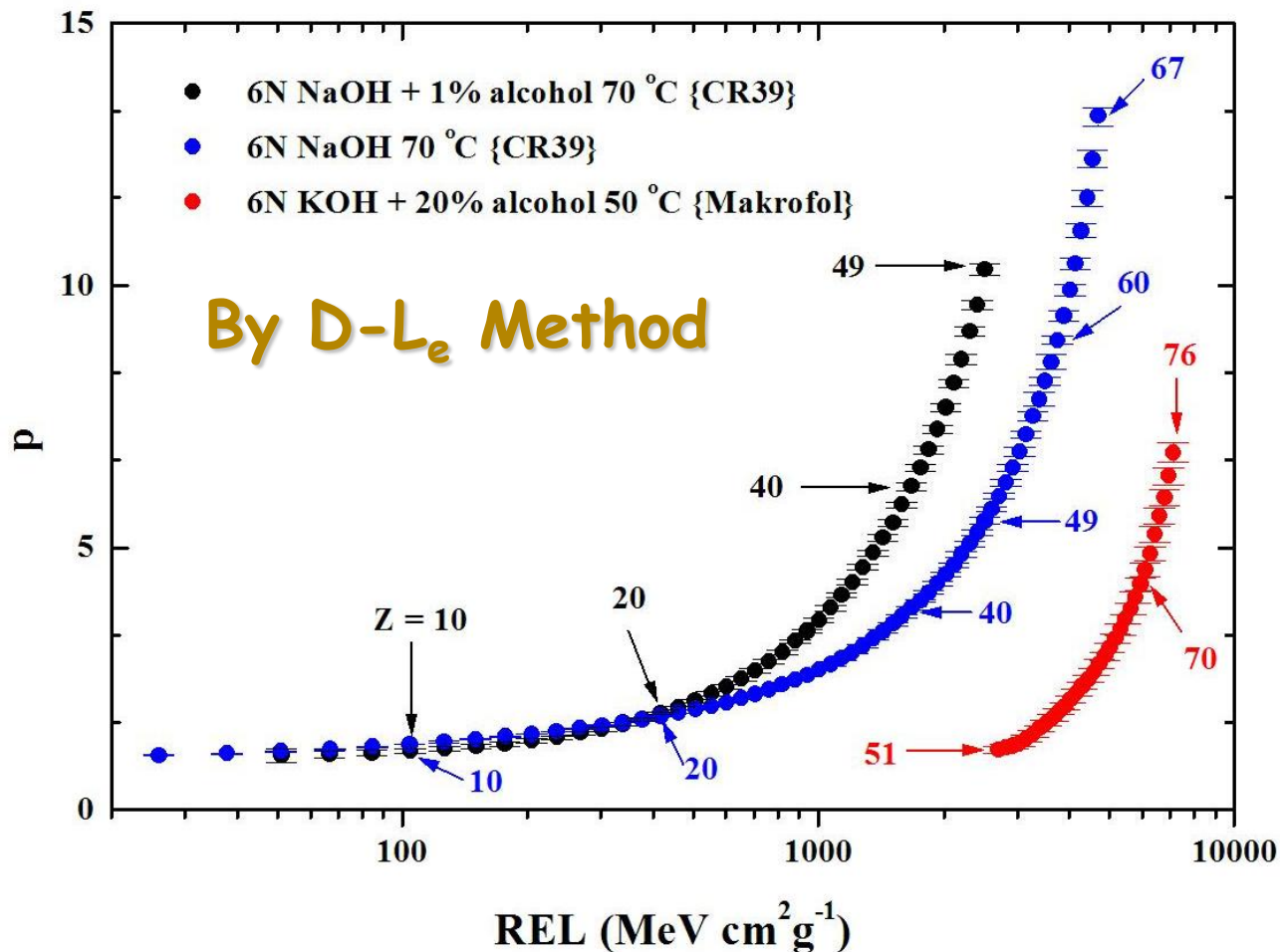
contd...

- The computer system attached with the microscope is installed with image processing software Leica QWin Plus for the study of track-images captured by CCD camera for gathering useful information or data for further analysis. Leica QWin Plus is a modular image processing and analysis software package with versatile architecture, designed to solve the demanding quantitative analysis tasks.
- It provides several classes of measurement ranging from interactive manual measurements of objects to fully 'hands-off' analysis. It provides access to menus and dialogues and works on Quips-routines (programs) developed for the desired purpose. Various parameters can be measured using Leica QWin Plus. e.g. length, area, x and y position, roundness, centroid, perimeter, equivalent diameter, counts, gray level, brightness etc.

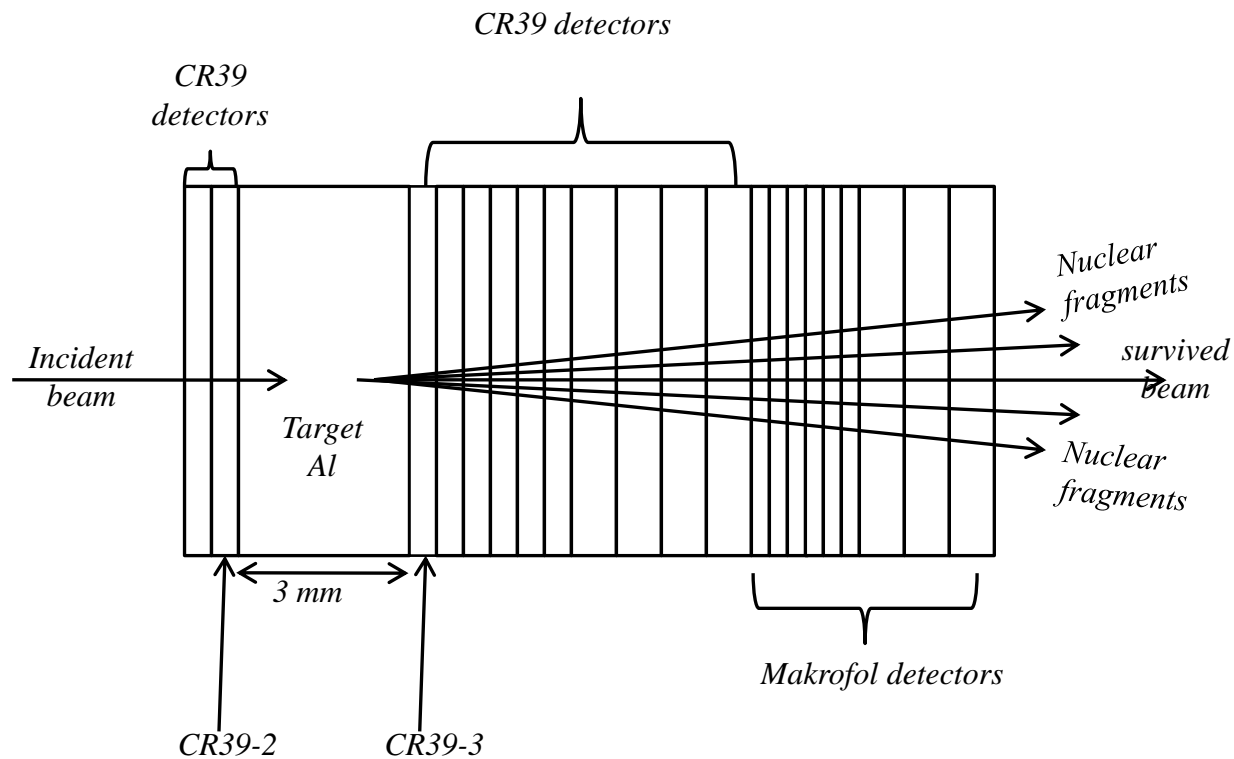
CALIBRATION GRAPH FOR CR39



RESPONSE CURVES FOR CR39 AND MAKROFOL



Comparison for CR39 NTDs exposed to 158 A GeV In^{49+} and Pb^{82+} heavy ions and etched under different "soft" condition. Notice the p values at $Z = 40$ and 49 for two etching conditions for CR39. A sharp rise in sensitivity is evident for etching with small fraction of alcohol after $Z/\beta \geq 20$.



Sketch of the stack configuration used for the exposures to 300 A MeV Fe^{26+} ion beam.

Single Side Etching

- To increase the diameter of the tracks without creating holes in the detectors, etching was performed on a single side of the detectors by applying adhesive 'araldite' on the other side surfaces.*
- Single side etching does not allow the development of track cones from the other side of the detectors due to same ion and so, more etching can be performed on the same side.*

Total Charge Changing Cross-Section

- Total charge changing cross-section was calculated by the relation: $\sigma_{tot} = X_T \cdot \ln(N_i/N_s)$
where $X_T = \frac{A_T}{\rho_T \cdot t_T \cdot N_A}$
- Height distribution was fitted by multiple Gaussians using Root analysis software.
- By this fitting, number of survived ions was observed to be 250 cm^{-2} within confidence level of 99.9%.
- the value of total charge changing cross-section was calculated to be $(2694 \pm 142) \text{ mb}$.
- Calculated value of the total charge changing cross-section is in good agreement within the experimental errors with the experimentally calculated values by Webber et al. and Zeitlin et al.

Track-diameter measurements using Automatic image analyzer

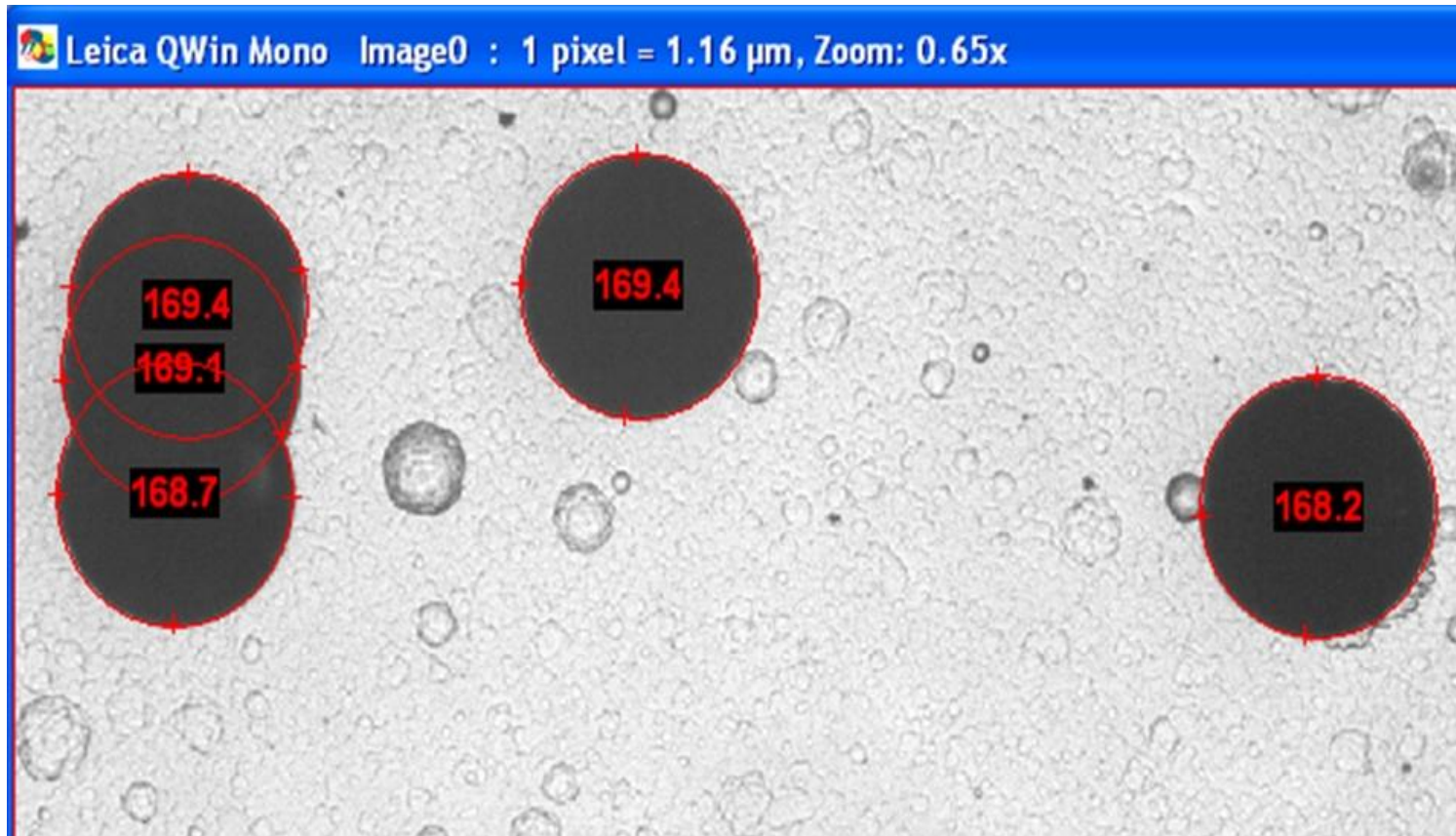
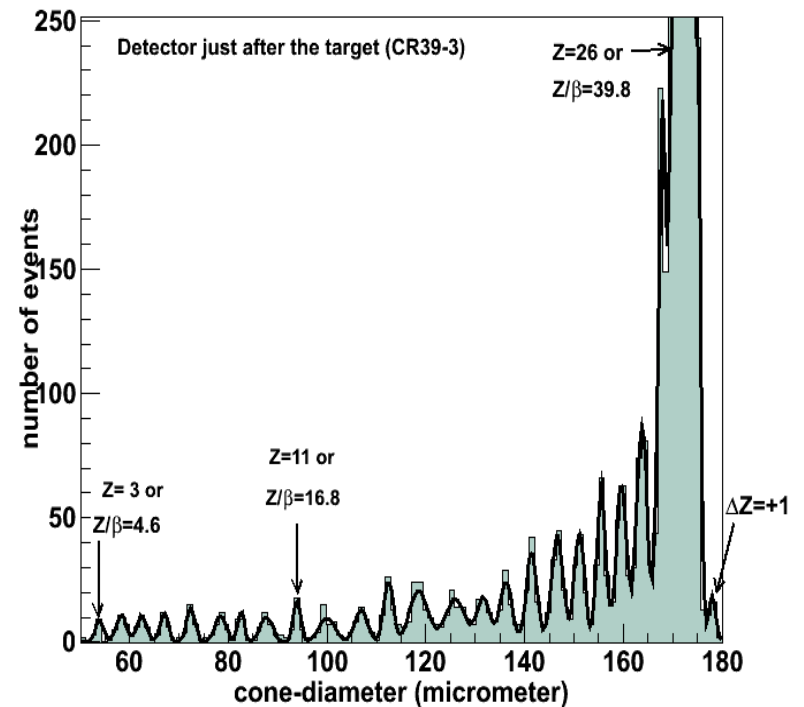
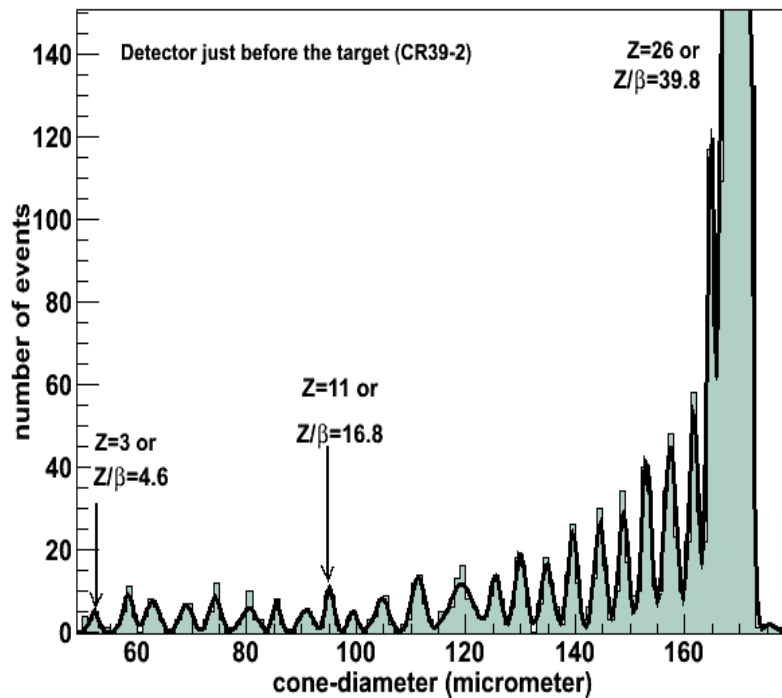
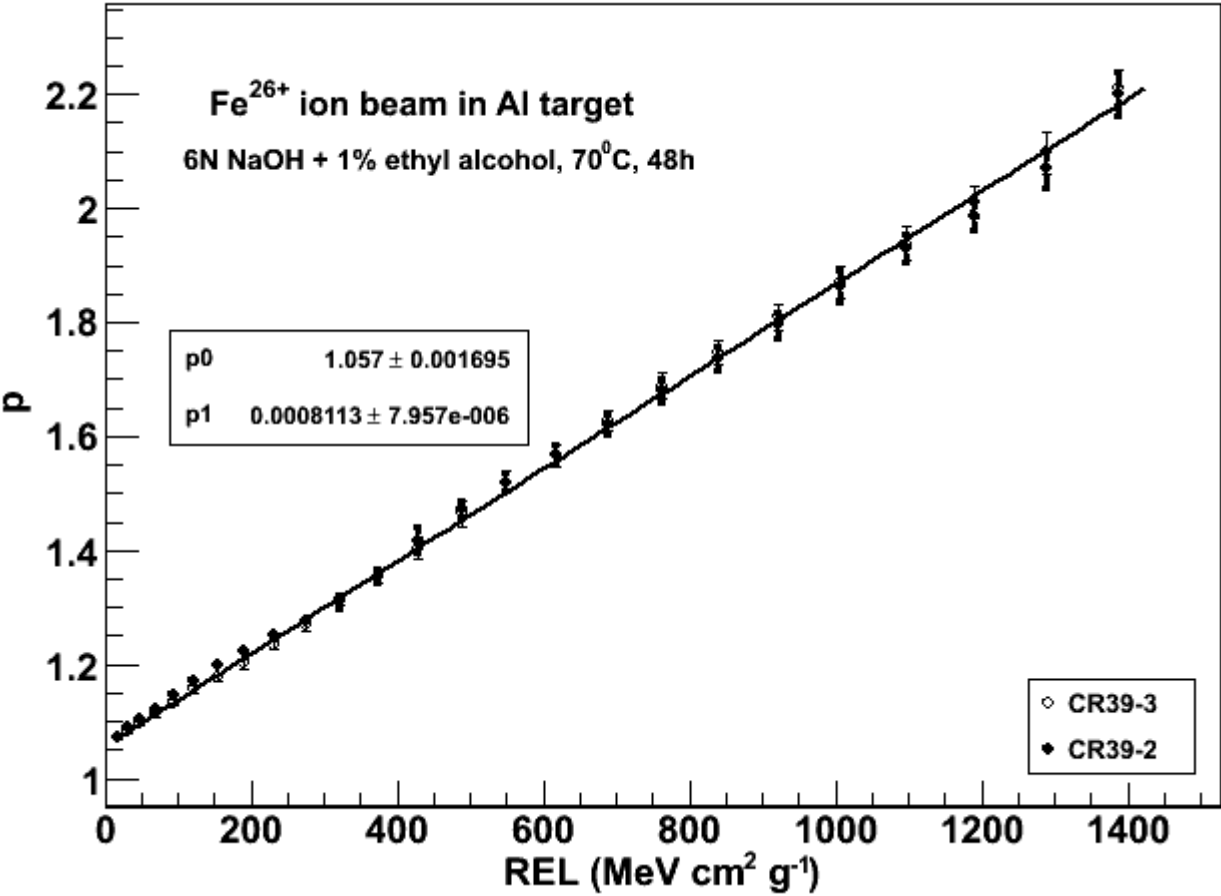


Image of a CR39 detector irradiated with 300 A MeV Fe^{26+} beam after etching of 48 hours

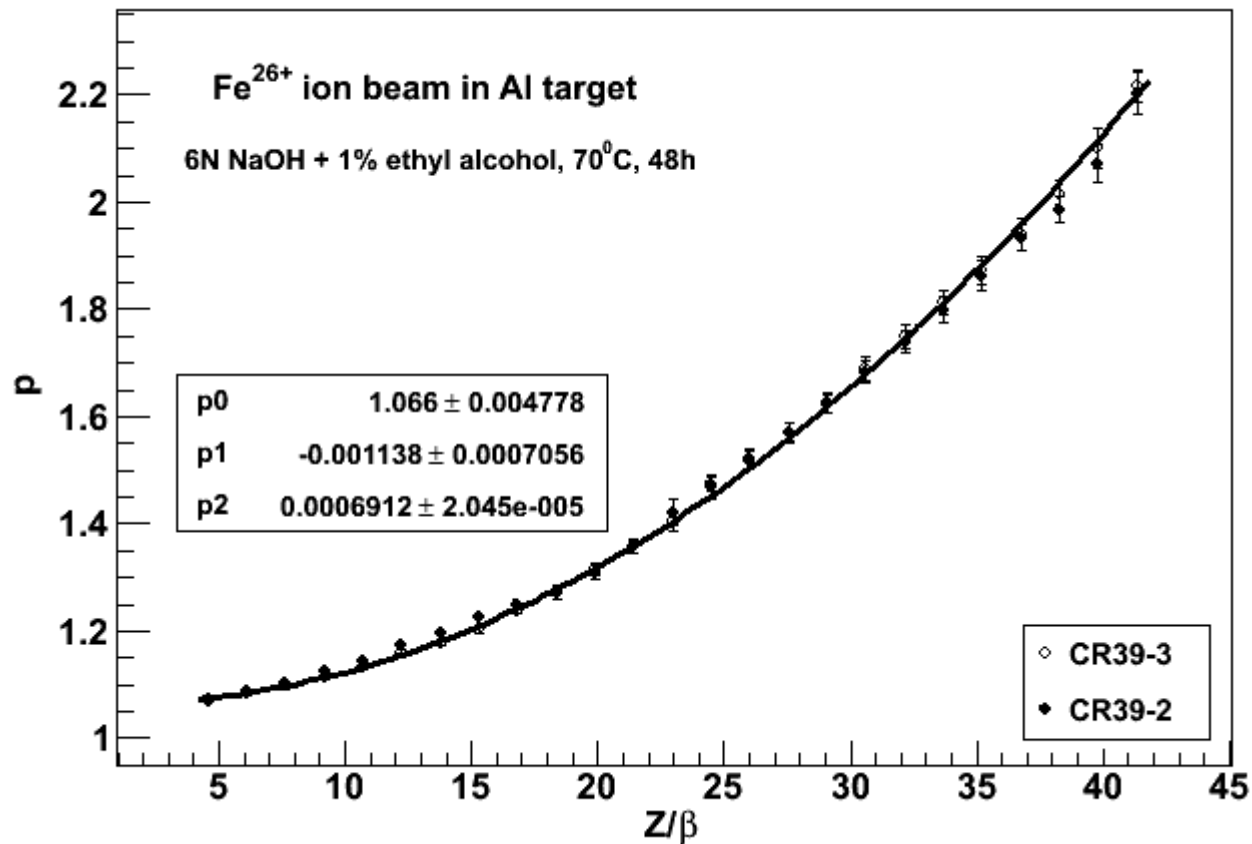
Cone diameter distribution of CR39 track detector exposed to 300 A MeV Fe^{26+} ion beam



Calibration curves (p vs REL) for CR39 detectors exposed to 300 A MeV Fe²⁶⁺ ion beam



Charge Response (p vs Z/β) of CR39 detectors for 300 A MeV Fe^{26+} ion beam



Total charge changing cross-section

- Total charge changing cross-section of 300 A MeV Fe^{26+} ion beam was experimentally calculated using the relation:

$$\sigma_{tot} = X_T \cdot \ln(N_i/N_s)$$

where $X_T = \frac{A_T}{\rho_T \cdot t_T \cdot N_A}$;

Atomic mass number and density of Al target materials are 27 and 2.692 g cm^{-3} respectively. Thickness of the target 0.3 cm. The value of total charge changing cross-section was calculated to be $\sigma_{tot} = (1663 \pm 236) \text{ mb}$

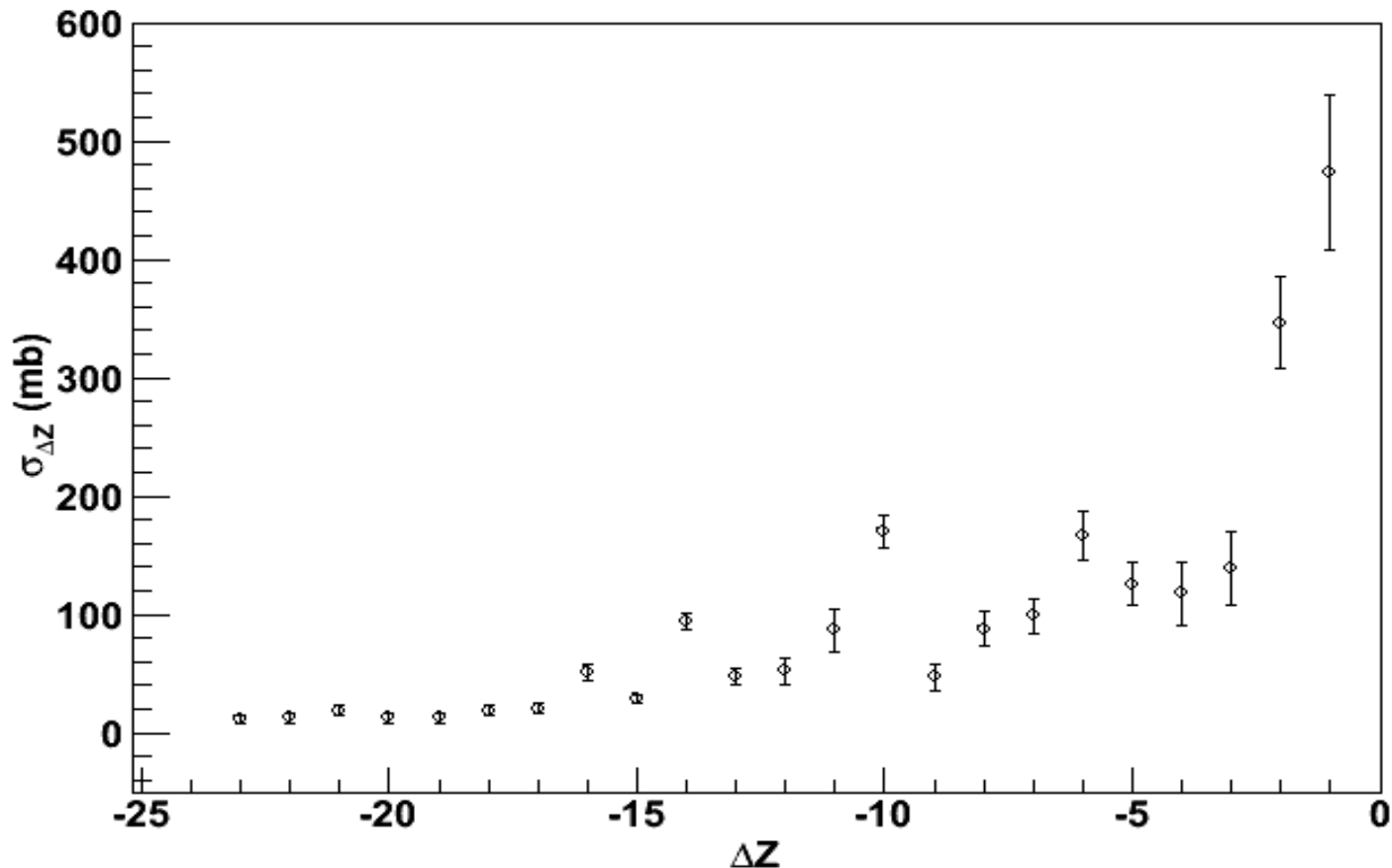
contd...

- The calculated cross-section was fitted to the Bradt-Peters geometrical cross-section for a projectile of mass number A_p on a target of mass number A_T using the relation*

$$\sigma = \pi r_0^2 \left(A_p^{1/3} + A_T^{1/3} - b \right)^2$$

where r_0 and b were 1.31 fm and 1.3 respectively. By taking A_p (= 56) for Fe as projectile and A_T (= 27) for Al as target, the geometrical cross-section is 1645 mb.

Partial Charge Changing Cross-Sections



Partial charge changing cross-sections of the fragments $\Delta Z = -23$ to -1 for 300 A MeV Fe^{26+} ion beam in Al target

Charge pick-up cross-section

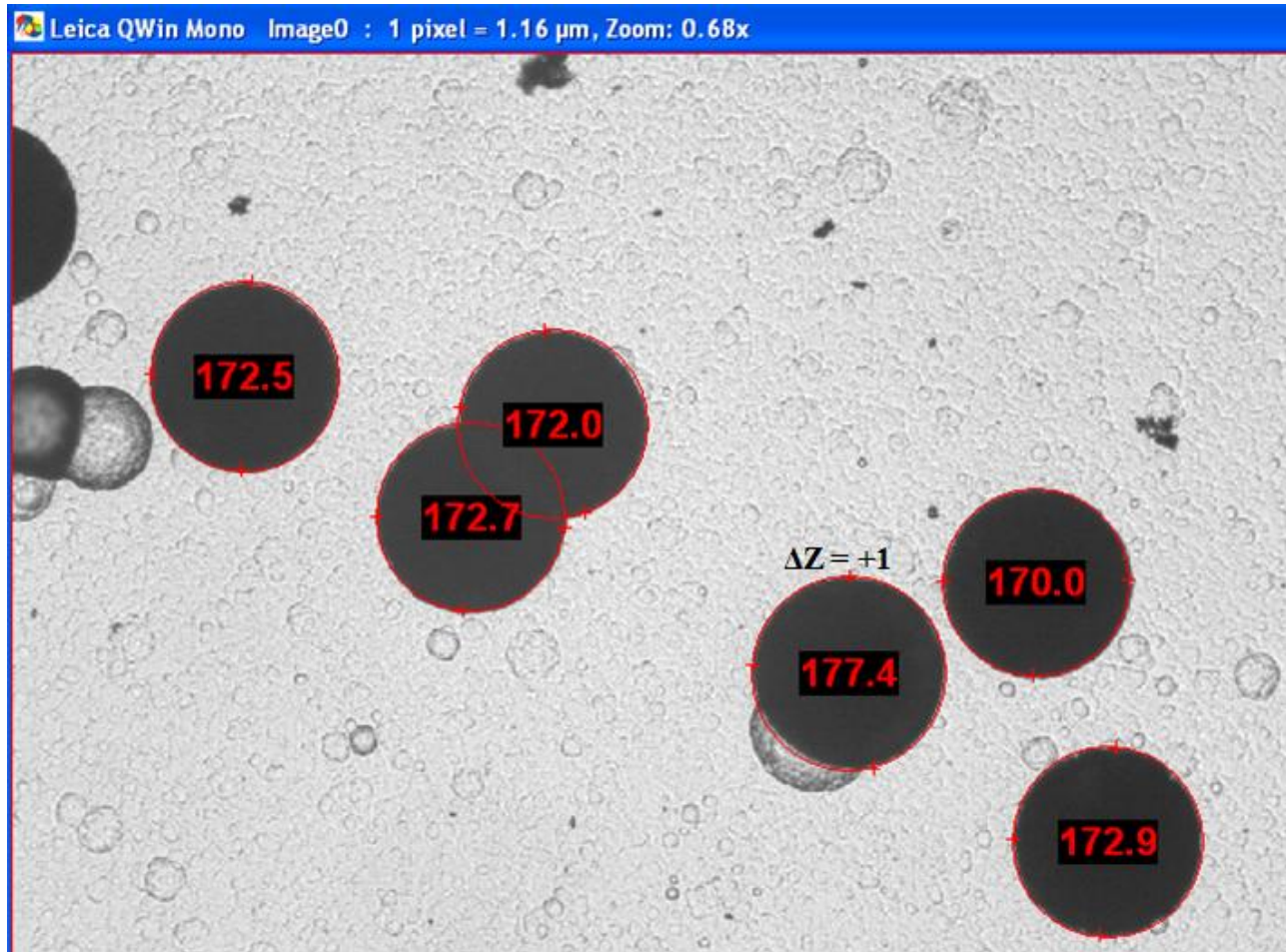


Image of tracks in the CR39-3 detector showing a charge pick-up event with

$\Delta Z = +1$ of diameter 177.4 μm .

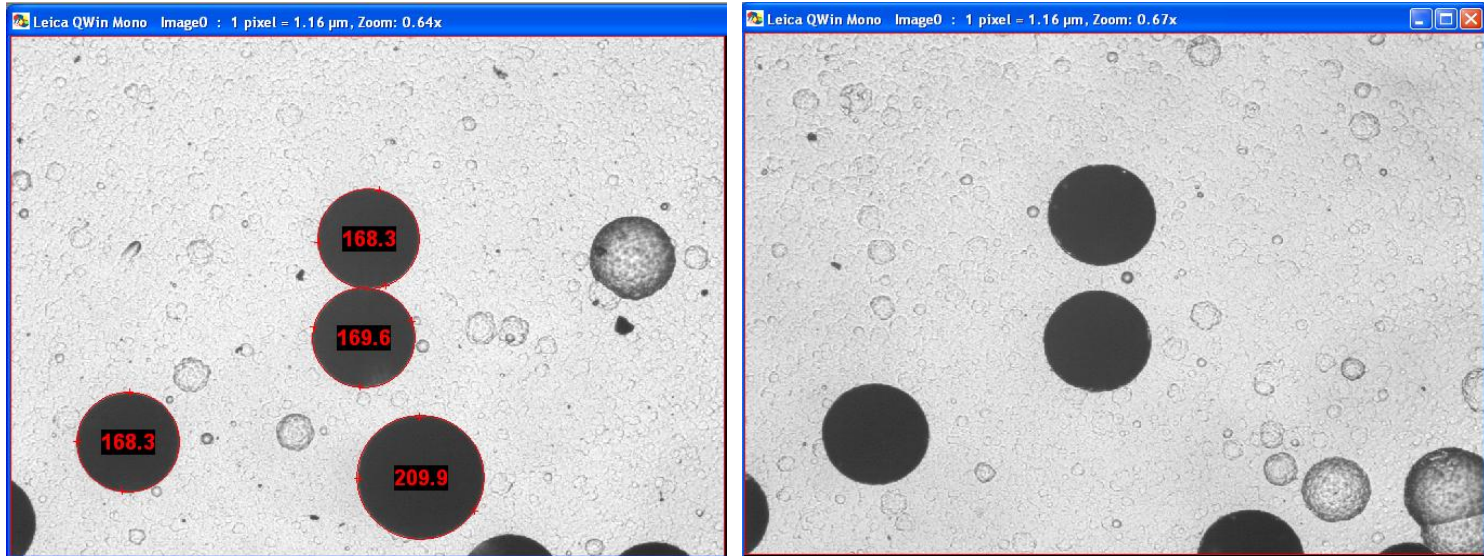
contd...

- *The charge pick-up cross-section was calculated by the formula*

$$\sigma = \frac{A}{N_A \rho t} \frac{N_{27}}{N_{beam}}$$

- *N_{27} is the number of charge pick-up events, N_{beam} is the number of beam particles exiting the target, A , ρ and t are the atomic mass number, density and thickness of the target respectively and N_A is Avogadro's number.*
- ***The charge pick-up cross section for $\Delta Z = +1$ was calculated: (92 ± 6) mb.***

Beam Contamination



(a)

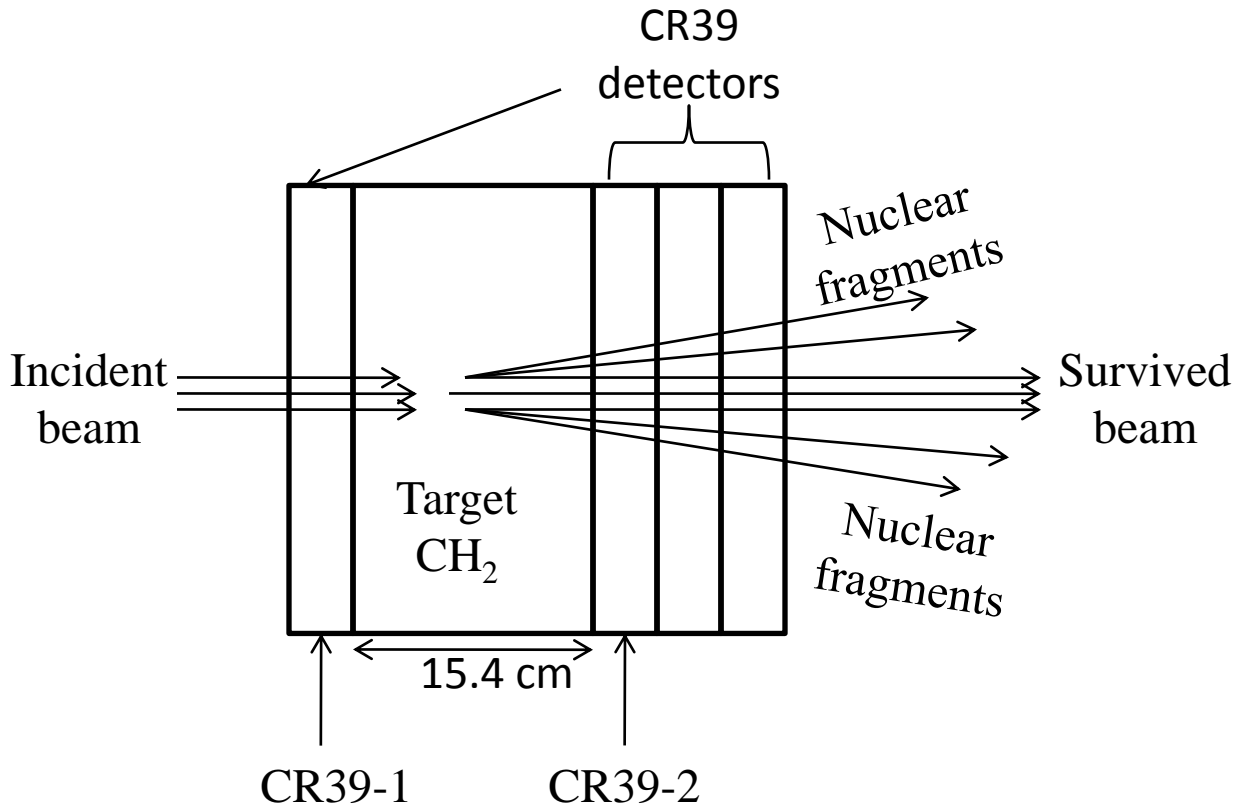
(b)

Fig. (a) Image of CR39-2 detector shows a contaminated track of diameter 209.9 μm whereas (b) Image of CR39-3 at the same position shows the absence of the contaminated track.

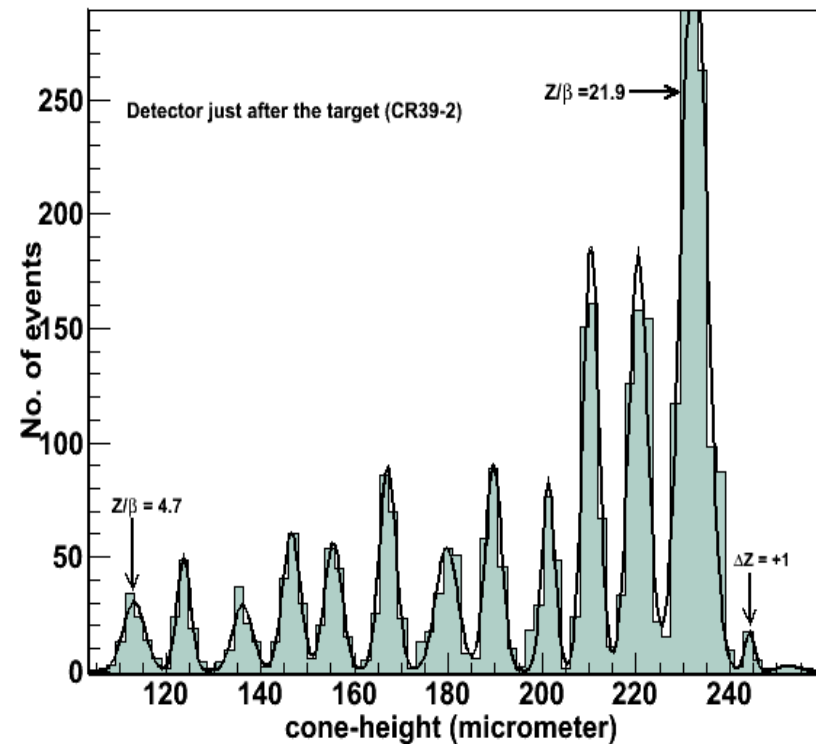
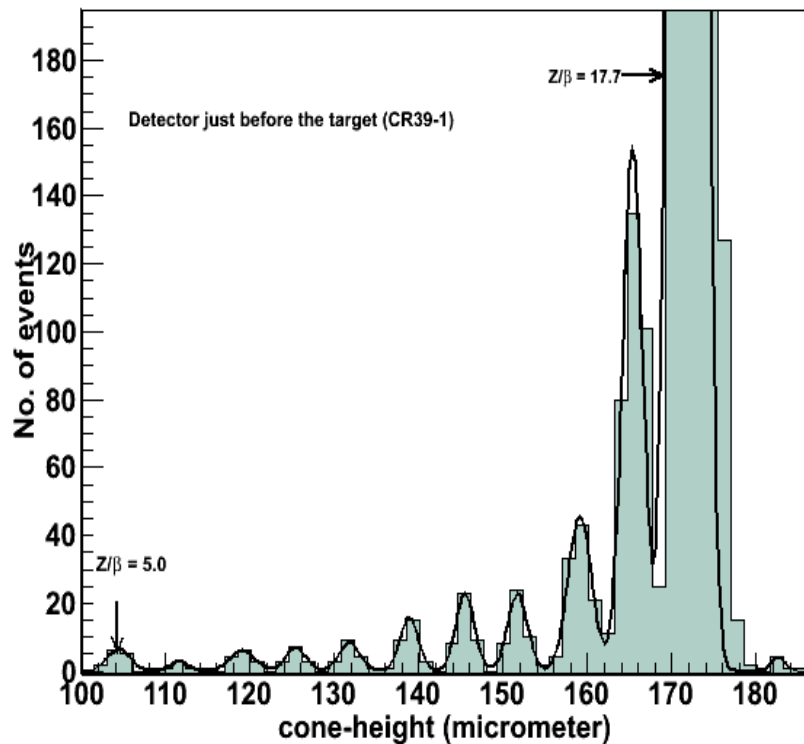
contd...

- Fig. (a) shows a track of diameter $209.9 \mu\text{m}$ in CR39-2 detector and Fig. (b) shows the absence of the same track in CR39-3 detector.
- There is an abrupt increase in the diameter. This track was present in the lower surface of CR39-2 detector but not present in CR39-3 detector. This means that this track could be due to some low energy particle. Such low energy particles may be due to some target fragment or fragment due to beam pipe scraping or interactions in the gas or other upstream matter .
- After scanning an area of $\sim 12 \text{ cm}^2$, it was found that about 0.04% tracks were due to particles with different charge or velocity from the beam particles.

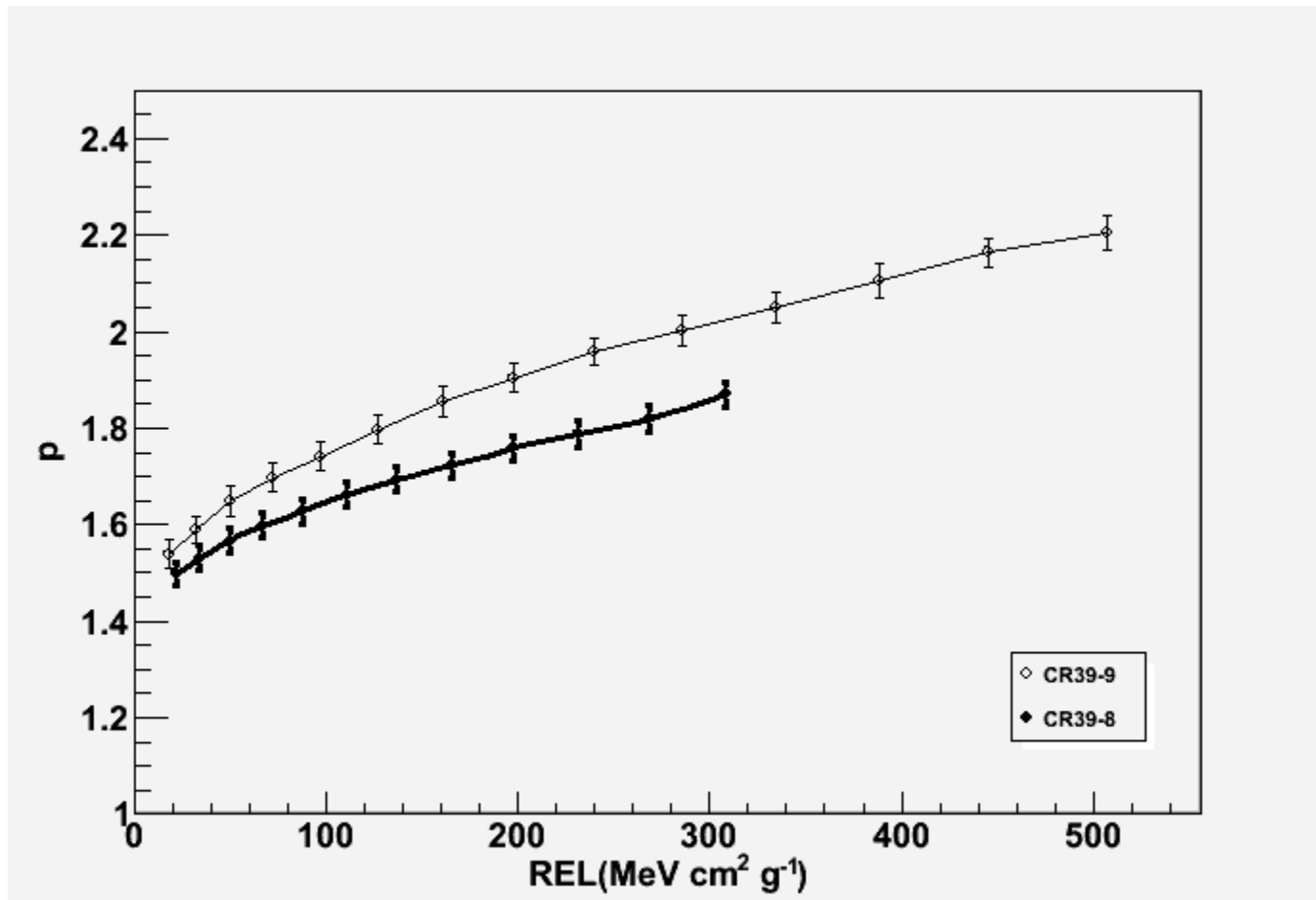
Sketch of the stack configuration used for the exposures to 600 A MeV Si^{14+} ion beam



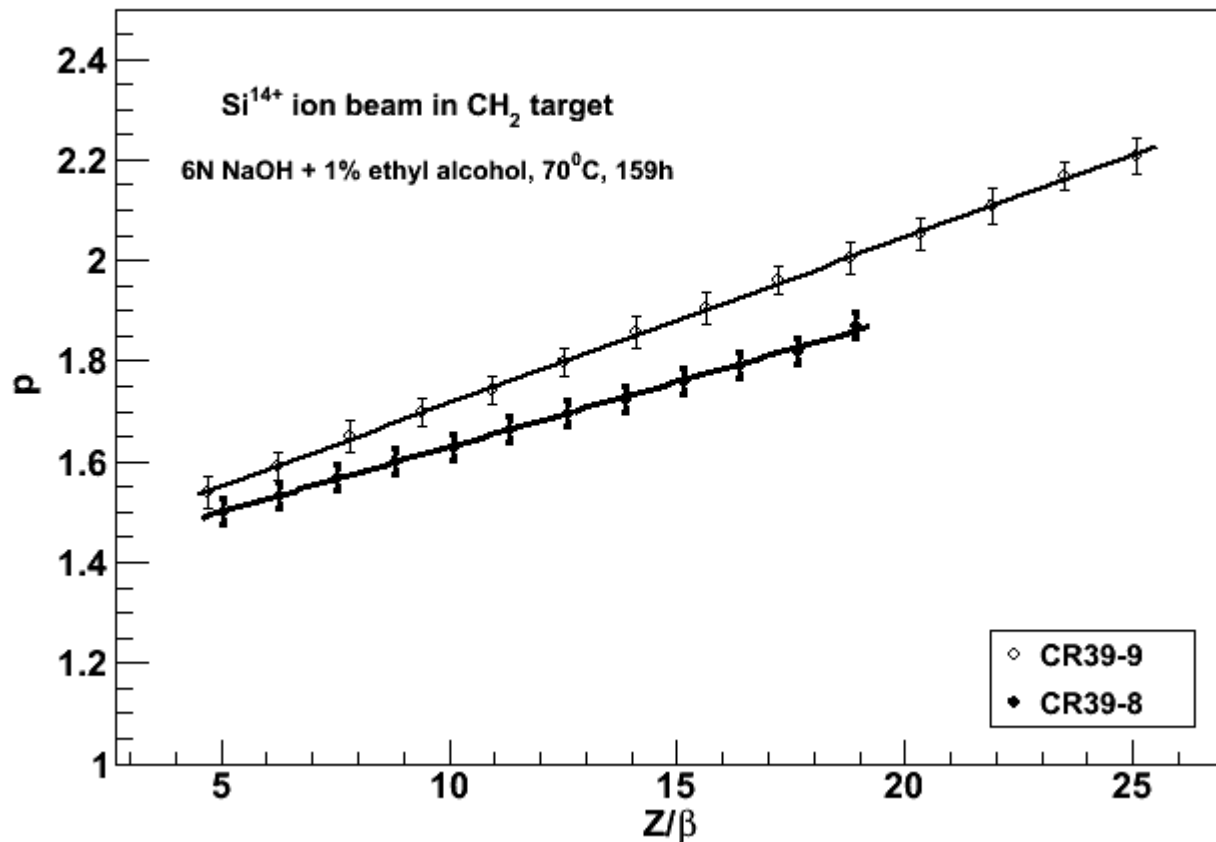
Cone-Height distribution of CR39 track detector exposed to 600 A $MeV Si^{14+}$ ion beam



Calibration curves (p vs REL) of CR39 detectors for 600 A MeV Si¹⁴⁺ ion beam



Charge response of CR39 detectors: CR39-1 and CR39-2 exposed to 600 A MeV Si¹⁴⁺ ion beam



Total charge changing cross-section

- Total charge changing cross-section of 600 A MeV Si¹⁴⁺ ion beam was experimentally calculated using the relation:

$$\sigma_{tot} = X_T \cdot \ln(N_i/N_s)$$

where

$$X_T = \frac{A_T}{\rho_T \cdot t_T \cdot N_A} ;$$

Atomic mass number and density of CH₂ target materials are 4.7 and 0.958 g cm⁻³ respectively. Thickness of the target 15.4 cm. The value of total charge changing cross-section was calculated to be (766 ± 17) mb

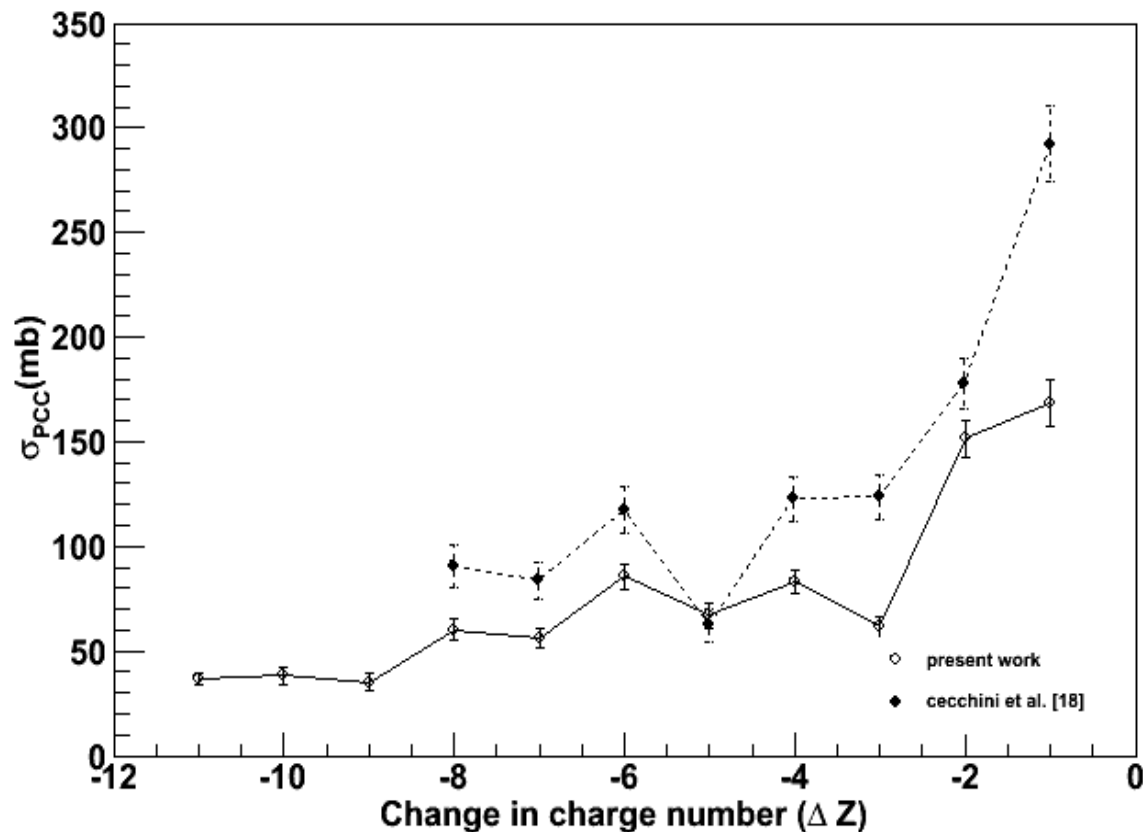
contd...

- The calculated cross-section was fitted to the Bradt-Peters geometrical cross-section for a projectile of mass number A_p on a target of mass number A_T using the relation*

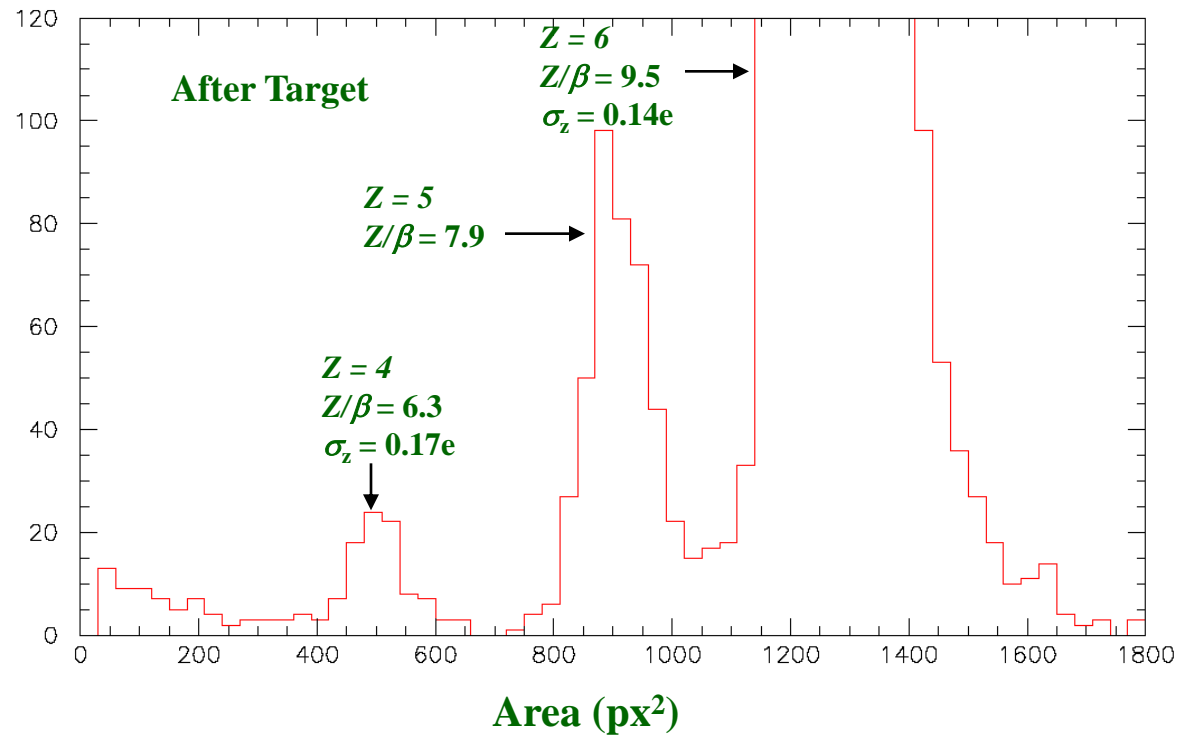
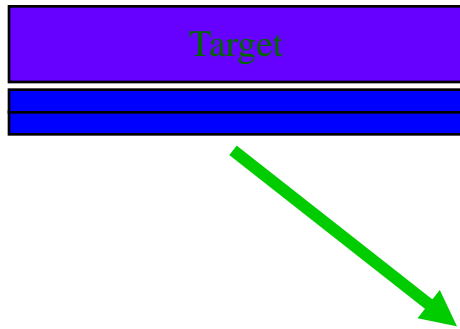
$$\sigma = \pi r_0^2 \left(A_p^{1/3} + A_T^{1/3} - b \right)^2$$

where r_0 and b were 1.31 fm and 0.94 respectively. By taking A_p (= 28) for Si as projectile and A_T (= 4.7) for CH_2 as target, the geometrical cross-section is 766 mb.

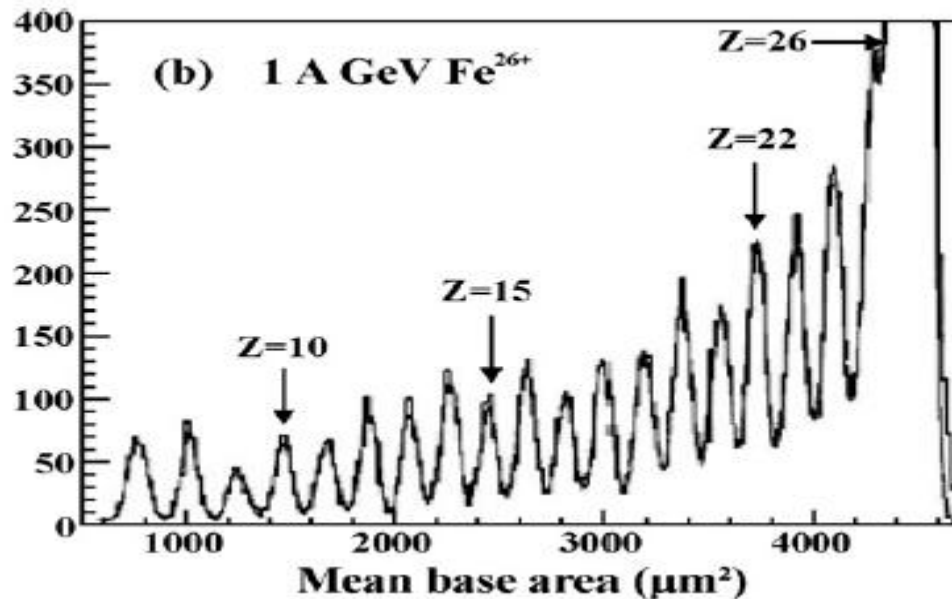
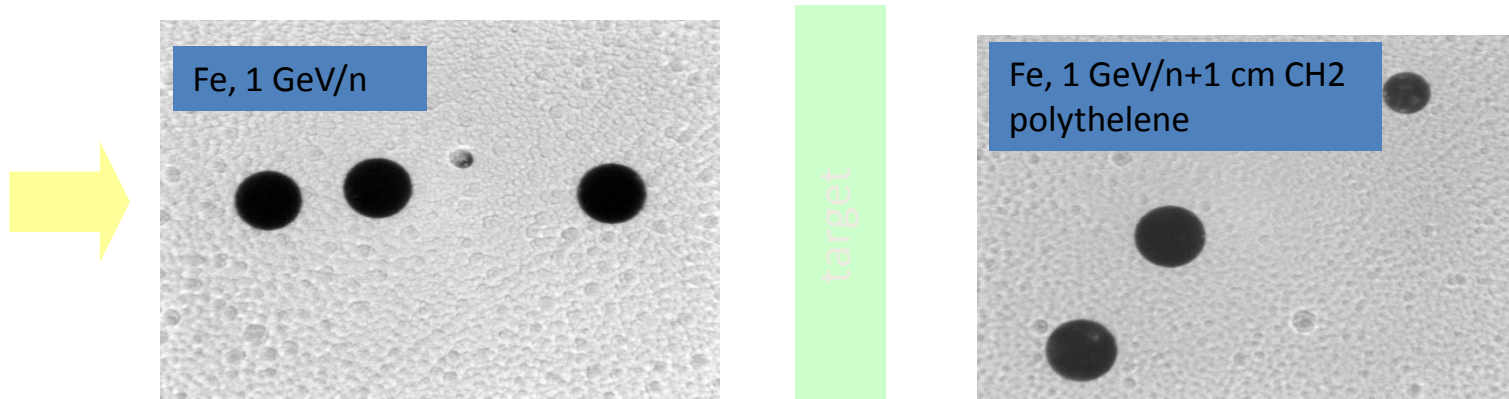
Partial charge changing cross-section (in mb) and a comparison with the earlier results



0.29 A GeV C + CH₂ (0.935 g/cm²)



Cross section measurements (“thin” target)



INTERCAST CR39

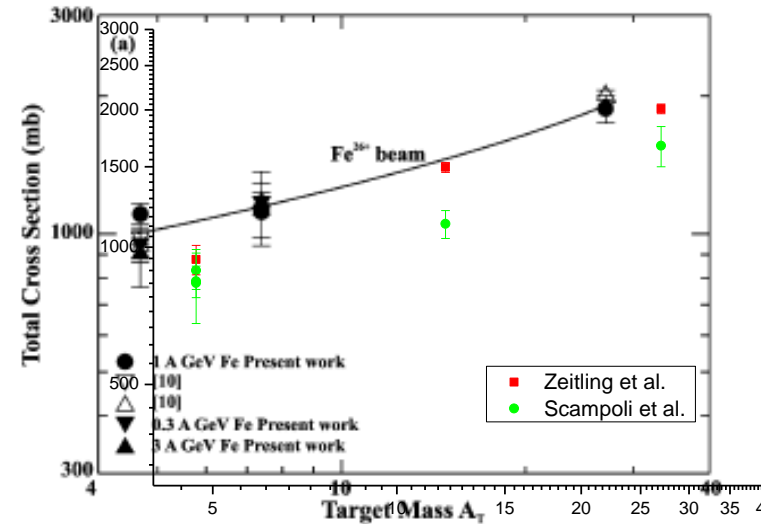
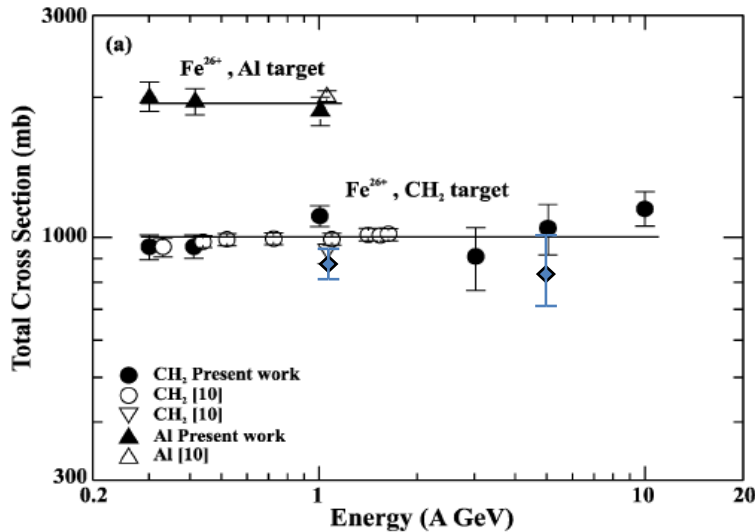
Etching condition:

6 N NaOH water solution

t=30 h

T=70°C

Cross section measurements



Cecchini S. et al., *Nucl. Phys.*, 2008

Database:

Ion	Energy range	Target
6C ; ^{28}Si ; ^{56}Fe ; ^{82}Pb	0.2 – 10 A GeV	CH_2 ; CR39; C; Al; Cu; Pb

Summary

- **Geant4 is one of the best simulation tool kit for the studies of heavy ions**
- **Calibrations of detectors are necessary for code bench marking, both in Space radiation-protection and radio-therapy with heavy ions like C, Si, Fe, Pb etc.**
- **Development of technology specially automatic image analyzer make more suitable track-etch detectors for future planning of hadrontherapy**
- **A unique method of one-side etching was used to avoid shadow effects occurring in cone-height measurements and through holes due to high Z fragments in the detector.**
- **Peaks due to fragments and beam ions were sharply resolved by the method based on the measurements of cone-height of tracks in single detector.**
- **The partial charge changing cross-section were calculated and a clear odd-even effect is also observed.**
- **The charge pick-up cross sections for $\Delta Z = +1$ and $\Delta Z = +2$ were calculated. It is also concluded that the charge pick-up cross section increases at lower energies.**
- **Clear contamination events (~0.04%) were observed. Dissociation events were also observed.**
- **Hadrontherapy could be best possible way for cancer treatment; specially for brain tumor, nearby spinal cord region and other sensitive human organs after proper simulation studies**
- **Shielding design could be better after simulation studies.**

Acknowledgements

- The author is thankful to the Department of Science & Technology, SERC division for financial assistance under the Research & Development project No. SR/S2/HEP-10/2009. The author is also thankful to my research scholars Mr. Summit Jalota and Ms. Renu Gupta for their contributions. Finally, author is grateful to Prof. Giorgio Giacomelli, Dr. Laura Patrizii, Dr. Vincent Togo from University of Bologna and INFN Bologna for their continuous support for this work.

Recent Publications by our group

- ***Simulation of depth-dose distributions for various ions in polyethylene medium***
Ashavani Kumar, Summit Jalota and Renu Gupta
Advances in Space Research 49 (2012) 1691.
- ***Validation of Geant4 physics models for 56Fe ion beam in various media***
Summit Jalota and Ashavani Kumar
Nucl. Instrum. & Meth. B 291 (2012) 7.
- ***Response of CR39 track etch detector to 10 A GeV Fe²⁶⁺ ion beam and total charge changing cross-section measurement***
A. Kumar, R. Gupta, S. Jalota, G. Giacomelli, L. Patrizzii, V. Togo
Nucl. Instrum. Methods B 270 (2012) 55.
- ***Measurement of Total and Partial Charge Changing and Charge Pick-up Cross-Sections for 300 A MeV Fe²⁶⁺ beam in Al with a new system of analysis***
R. Gupta, A. Kumar, G. Giacomelli, L. Patrizzii, V. Togo
Nucl. Instrum. Methods A 694 (2012) 32.
- ***Calibration of CR39 detectors with new system for Fe²⁶⁺ ion beam and measurement of total charge changing cross-section in Al Target***
R. Gupta, A. Kumar, G. Giacomelli, L. Patrizzii, V. Togo
Radiat. Meas. 47 (2012) 1023.

Published Papers in the Field:

- Journal of computational physics 233 (2013) 464.
- Nucl. Instr. and Meth. B 268 (2010) 2343.
- Nuclear Physics A 784 (2007) 341.
- Nucl. Instr. and Meth. B 254 (2007) 254.
- Nuclear Physics B (Proc. Suppl.) 172 (2007) 92.
- Nucl. Instr. and Meth. A 453 (2000) 525.
- Nucl. Phys. A 807 (2008) 206.
- Nucl. Instr. and Meth. A 580 (2007) 58.

- **C. Zeitlin, J. Miller, L. Heilbronn et al., “The fragmentation of 510 MeV/nucleon iron-56 in polyethylene. I. Fragment fluence spectra”. Rad. Res. 145, 655-665 (1996)**
- **TT Bohlen, F. Cerutti, M. Dosanjh et al., Benchmarking nuclear models of FLUKA and GEANT4 for carbon ion therapy. Phys. Med. Bio. 55, 5833-5847 (2010).**
- **C. Lobascio, M. Briccarello, R. Destefanis et al., Accelerator-based tests of radiation shielding properties of materials used in human space infrastructures. Health Phys. 94, 242-247 (2008).**
- **M. Silvestri, E. Tracino, M. Briccarello et al., Impact of spacecraft-shell composition on 1 GeV/nucleon ^{56}Fe ion-fragmentation and dose reduction. 58, 3126-3133 (2011).**
- **C. Zeitlin, A. Fukumura, L. Heilbronn et al., Fragmentation cross sections of 600 MeV/nucleon ^{20}Ne on elemental targets, Phys. Rev. C. 64, 024902 (2001).**
- **W. R. Webber, J. C. Kish, D. A. Schrier. Individual charge changing fragmentation cross section of relativistic nuclei in hydrogen, helium and carbon targets, Phys. Rev. C. 41, 533-546 (1990).**
- **L. W. Townsend, F. A. Cucinotta, L. H. Heilbronn, Nuclear model calculations and their role in space radiation research, Adv. Space Res. 30, 907-916 (2002).**
- **M. Durante, Physical basis of radiation protection in space travel, Rev. Mod. Phys. 83, 1245-1281 (2012).**
- **F. Flesch, G. Iancu, W. Heinrich, H. Yasuda, Projectile fragmentation of Silicon ions at 490 A MeV, Rad. Meas. 34, 237-240 (2001).**
- **Brechtmann, C., Heinrich, W., 1988. Measurements of elemental fragmentation cross section for relativistic heavy ions using CR-39 plastic nuclear track detectors. Nucl. Instrum. Methods B. 29, 675–679.**

Thank you